A Critical Evaluation of Moment Gradient (C_b) Factor Calculation Procedures for Singly Symmetric I-Section Members

Ryan Slein, Woo Yong Jeong, and Donald W. White

ABSTRACT

This paper explores the manual calculation of the elastic lateral-torsional buckling resistance of prismatic singly symmetric I-section members having a variation in the bending moment between the brace points. The paper shows that the quarter-point moment gradient factor, C_b, equation in the AISC *Specification* (2016), as modified by its Commentary, is inaccurate for reverse-curvature bending of singly symmetric I-section members. The modified equation cannot accurately represent the behavior for reverse-curvature bending of singly symmetric members in general because it is blind to the sign of the bending moment. That is, it does not recognize the influence of different patterns of compression and tension in the different size flanges. Furthermore, the AISC *Specification* Commentary (ASC) calculation exhibits substantial discontinuities in its C_b values as a function of the loading considered. This is due to the application of a modifier, termed R_m, creating a step-function behavior that gives substantially conservative results in certain situations and substantially unconservative results in other cases.

In addition, the paper explains that the C_b equations in the current AASHTO *Specifications* (2020) provide some accounting for the different patterns of compression in the separate flanges for cases involving moment reversal. However, these equations are based only on the moments at the ends and at the middle of the unbraced length. Hence, they are limited in their ability to capture the influence of nonlinear variations in moment along the unbraced length. Furthermore, the AASHTO procedure uses $C_b = 1.0$ when the moment within the unbraced length is larger than the maximum brace point moment, causing compression in the flange under consideration (in single- or reverse-curvature bending). This practice can result in substantial conservatism. AASHTO recommends other methods such as the ASC approach in these cases. Lastly, the AASHTO C_b values can exhibit substantial discontinuities as a function of the loading considered. This is due to changes in the governing flange in the AASHTO procedure. This attribute also produces substantially conservative results in certain cases.

To rectify the limitations of the ASC and AASHTO methods, the paper recommends a modified form of an alternative quarter-point C_b equation proposed by Wong and Driver (2010). For singly symmetric cases involving moment reversal, the terms in the quarter-point equation are replaced by the ratio of the moments to the corresponding elastic buckling moment based on $C_b = 1$, considering which flange is in compression at each of the locations where the moments are sampled. The studies show that the Wong and Driver equation, with this modification, provides substantially improved accuracy compared to the existing AASHTO and ASC equations for reverse-curvature bending with slightly less calculation effort. In addition, the paper demonstrates the accuracy of the direct application of the Wong and Driver equation for single-curvature bending cases.

Keywords: lateral-torsional buckling, moment gradient, singly symmetric I-section members.

INTRODUCTION

Singly symmetric welded I-section members are widely employed for optimized member designs due to their structural efficiency. In the AISC *Specification for Structural Steel Buildings* (2016) and the AASHTO *LRFD Bridge Design Specifications* (2020), the lateral-torsional buckling (LTB) resistance of unbraced lengths subjected to moment gradient is determined by multiplying the LTB resistance for uniform bending by the moment gradient factor C_b. The resistance is capped by the "plateau strength" of the member in flexure (equal to the plastic moment, M_p, for compact web I-section members, and equal to the yield moment of the compression flange multiplied by the bending strength reduction factor, $R_{pg}M_{yc}$, for slender-web members).

To determine the LTB resistance accurately under moment gradient loading, it is important to calculate an accurate C_b. The C_b factor is influenced generally by:

1. The shape of the moment diagram between the braced points.
2. The extent of the monosymmetry of the cross section.
3. The length-to-depth ratio and cross-section dimensions,

Ryan Slein, Research Affiliate, Georgia Institute of Technology, Atlanta, Ga. Email: ryan.slein@gatech.edu; ryan.slein@dot.gov

Woo Yong Jeong, Senior Software Lead, HEXAGON (GT STRUDL), Email: wooyong.jeong@hexagon.com

Donald W. White, Professor, Georgia Institute of Technology, Atlanta, Ga. Email: don.white@ce.gatech.edu (corresponding)

Paper No. 2018-05R2

which influence the relative contribution of the St. Venant and warping torsional stiffnesses to the LTB resistance.

4. The elevation of the applied load relative to the mid-height of the web.
5. The degree of lateral, rotational, and warping restraint at the ends of the unbraced lengths (including continuity with and buckling interaction with adjacent unbraced segments).

Steel design specifications typically simplify their calculation procedures by considering only item 1 or items 1 and 2 in the calculation of C_b and by considering items 2 and 3 in the base calculation of the elastic LTB resistance. For slender-web members, AISC (2016) and AASHTO (2020) set the St. Venant torsion constant, J, to zero to account for the influence of web distortion. Transverse load-height effects typically are neglected. Helwig et al. (1997) provide a thorough discussion of when this simplification is and is not appropriate. In addition, warping and minor-axis rotations are assumed unrestrained at the ends of member unbraced lengths, and the influence of continuity with adjacent unbraced lengths (typically referred to as interaction buckling) is neglected. For this reason, this paper evaluates manual C_b calculations that consider only the influence of item 1 for single-curvature bending, and include both items 1 and 2 for reverse-curvature bending. Comparisons are made to benchmark elastic LTB numerical solutions that account for items 1, 2, and 3. These benchmark solutions are conducted with any transverse loads applied at the mid-height of the web. Helwig et al. show that this position, rather than the shear center, is the proper transverse load location for the development of base C_b equations that neglect load height. Helwig et al. find, for single-curvature bending cases, that the degree of monosymmetry does not affect the C_b values and also that the base C_b values derived for doubly symmetric members work well when the load position is defined at the web mid-height rather than the shear center. Downward transverse loads applied at a location above the web mid-height cause destabilizing effects, and downward transverse loads applied at a location below the web mid-height cause stabilizing effects. Helwig et al. recommend a simple adjustment to the base C_b equations that gives a coarse approximation of load height effects, and they discuss in detail when these effects need or do not need to be included in design calculations.

Studies of the moment gradient factor, C_b, often have emphasized cases where the entire span is unbraced and subjected to applied transverse loads and the end moments are based on ideally pinned or fixed boundary conditions. While it is important to predict the LTB resistance in these cases, there is at least some bracing within the span in many situations. The moment diagrams within the individual unbraced lengths tend to be close to linear when only a few intermediate braces are provided. Furthermore, the moment diagrams for vertical members such as columns commonly are close to being linear. In addition, fixed end conditions are rare in practice, typically occurring only due to symmetry of the loading and the geometry. In this study, a broad range of loadings are considered, producing both linear and near-linear moment diagrams as well as a range of end moments relative to the moments from transverse loading. The loading cases studied encompass and expand upon the loadings considered in the prior studies by Helwig et al. (1997) and Wong and Driver (2010).

While the AASHTO (2020) C_b equations apply to both doubly and singly symmetric I-section members, the AISC *Specification* (2016) provides only one equation for C_b and references its Commentary for the handling of single symmetry. This paper shows that the current AASHTO and AISC *Specification* Commentary (ASC) predictions of the LTB resistance for singly symmetric I-section members subjected to moment reversal are often poor. To address this problem, the paper investigates and demonstrates a modification of the Wong and Driver (2010) C_b equation that results in a significant improvement in the accuracy of the LTB assessment for a complete range of doubly and singly symmetric member design situations while maintaining simplicity of the calculations. In addition to addressing the challenges for reverse-curvature bending, the paper demonstrates the accuracy of the direct application of this equation for single-curvature bending cases. These gains are achieved with effectively no change in the overall calculation effort relative to the current methods.

BACKGROUND

Calculations of C_b for singly symmetric I-section members typically involve modifications or extensions of C_b equations developed for doubly symmetric members. Therefore, it is essential to understand several particulars of C_b estimates for doubly symmetric members when considering predictions involving single symmetry. Wong and Driver (2010) evaluated a broad range of approaches recommended in the literature for the calculation of C_b for doubly symmetric I-section members. They proposed a new quarter-point C_b formula that maintains simplicity of the design calculations and provides measurable improvements in overall accuracy relative to other methods in the literature, including the AISC (2016) and AASHTO (2020) C_b equations. Figure 1 compares the result from the Wong and Driver C_b equation to the corresponding AISC and AASHTO equations for the basic case of linear moment diagrams. The AASHTO equation, discussed subsequently, uses a maximum cap of 2.3 and was originally developed as a lower-bound fit to solutions from Salvadori (1956) for linear moment diagram cases. However, other references [e.g., Ziemian (2010)] have

employed a larger cap of 2.5 or 2.56 with this equation. The AASHTO equation with a cap of 2.5 is shown to provide an appropriate lower bound of benchmark C_b values for a comprehensive range of cases in Slein et al. (2021) and is thus employed in Figure 1. Wong and Driver (2010) also suggest a maximum cap of 2.5 on their equation, although they state that their equation produces good results without this limit. Slein et al. confirm this is the case. For linear moment diagrams, the Wong and Driver equation gives a maximum value of 2.41.

Figure 2 plots the ratio of the Wong and Driver equation and AISC *Specification* Equation F1-1 to the AASHTO equation for linear moment diagram cases. This paper demonstrates that the AASHTO equation with a maximum limit of 2.5 provides the most accurate (largest) lower bound of the equations considered for these types of moment diagrams. The Wong and Driver quarter-point equation provides a reasonable conservative estimate for this case. One can observe that the AISC equation, which is also a quarter-point formula, gives results as much as 5.0% conservative

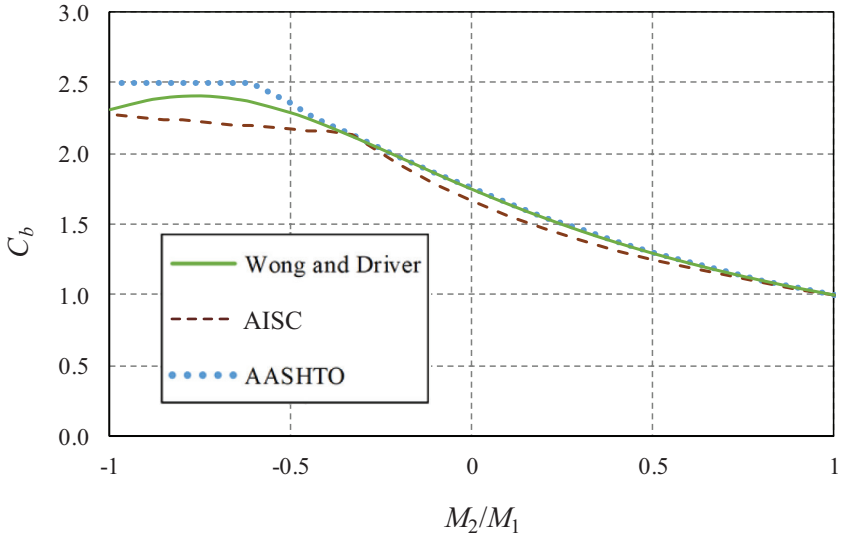

Fig. 1. Comparison of Wong and Driver, AISC, and AASHTO C_b *values versus the ratio of the smaller to larger end moments,* M_1/M_2*, for linear moment diagram cases.*

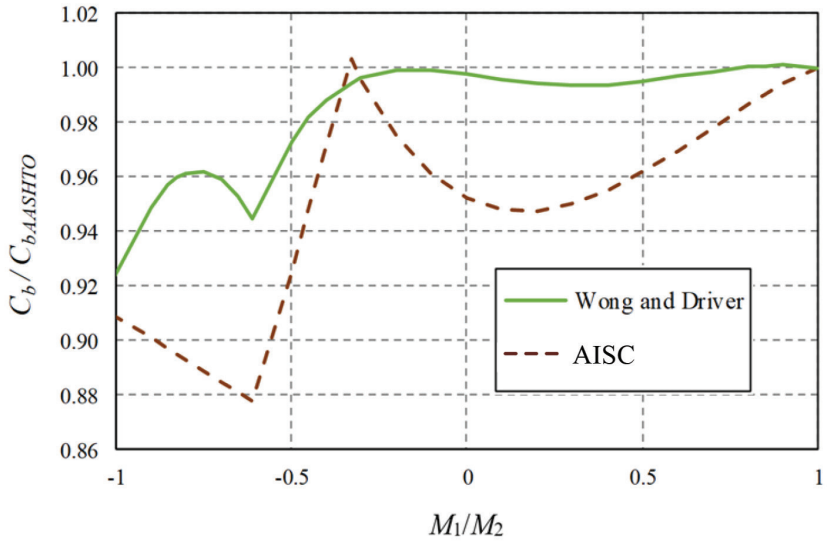

Fig. 2. Ratio of C_b *values from Wong and Driver and AISC to the AASHTO lower-bound* C_b *estimate versus the ratio of the smaller-to-larger end moments,* M_1/M_2*, for linear moment diagram cases.*

even for single-curvature bending (corresponding to a positive ratio of the smaller-to-larger end moments, M_1/M_2). For reverse-curvature bending cases, the AISC estimate can be as much as 12% conservative relative to the AASHTO lower-bound estimate.

Furthermore, Wong and Driver show that the AISC equation overestimates the C_b values from refined benchmark solutions for unbraced lengths containing a concentrated transverse load at the mid-length combined with restraining end moments as shown in Figure 3 when $0.6 < \beta < 1.1$, where β is the ratio of the actual end moments to the end moments for a fixed-end beam. They find that the largest unconservative error occurs for the case with $\beta = 1.0$. For this case with $\beta = 1.0$, the quarter-point Equation F1-1 in the AISC *Specification* gives $C_b = 1.92$, whereas benchmark solutions in this research range from 1.69 to 1.72, depending on the relative contributions from St. Venant and warping torsion. The proposed Wong and Driver formula gives $C_b = 1.41$, whereas the AASHTO procedure conservatively gives $C_b = 1.0$ for this problem.

While these improvements are relatively minor, they are measurable, and they provide specific reference points indicating that the Wong and Driver equation may also serve as a more appropriate base than the AISC *Specification* Equation F1-1 for the estimation of moment gradient effects in the context of singly symmetric I-section members.

The following subsections summarize the particulars of the AISC *Specification* Commentary (ASC), AASHTO, recommended, and benchmark calculations of C_b considered in this paper for singly symmetric I-section members. Appendix B provides a specific design example illustrating the relative efficiency of the ASC, AASHTO, and recommended calculations.

AISC *Specification* Commentary (ASC) Procedure

The AISC *Specification* Commentary (ASC) procedure uses the equation:

$$C_b = \left(\frac{12.5M_{max}}{2.5M_{max} + 3M_A + 4M_B + 3M_C}\right) R_m \leq 3.0 \quad \text{(AISC } \textit{Spec.} \text{ Comm. Eq. C-F1-3)}$$

where

M_A, M_B, M_C = absolute value of the moments at the quarter, middle, and three-quarter point locations, respectively, of the unbraced length, kip-in. (N-mm)

M_{max} = absolute value of maximum moment within the unbraced length, L_b, kip-in. (N-mm)

R_M = 1.0 (1a)

for doubly symmetric members and for singly symmetric members subjected to single-curvature bending, and

$$= 0.5 + 2\left(\frac{I_{y.opp}}{I_y}\right)^2 \quad (1b)$$

for singly symmetric members subjected to reverse-curvature bending, in which

I_y = weak-axis moment of inertia of the entire section, in.^{4} (mm^4)

$I_{y.opp}$ = moment of inertia of the flange on the opposite side of the web mid-height from the direction of the transverse loading, in.^{4} (mm^4)

Equation 1b is the same as Equation C-F1-4 in the ASC but with $I_{y.Top}$ labeled as $I_{y.opp}$. As stated in the ASC, Equation C-F1-4 was developed by focusing on gravity loading on horizontal beams. The ASC indicates that for general cases, such as columns subjected to transverse loads, the "top" flange is defined as the flange on the opposite side of the web mid-height from the direction of the transverse loading. The notation $I_{y.opp}$ is employed in this study to avoid any confusion regarding the reference to the "top" and "bottom" flanges.

In the ASC procedure, when the unbraced length is subjected to reverse-curvature bending, C_b is first calculated from the ASC Equation C-F1-3 and Equation 1b. It is then applied to the separate elastic LTB resistances under uniform bending, M_{cr1}, corresponding to flexural compression in each of the flanges to estimate the maximum moment, causing flexural compression in the given flange, at incipient elastic LTB. The corresponding elastic buckling load ratio may be written as:

$$\gamma_{eLTB} = \min\left(\frac{C_b M_{cr1.top}}{M_{max.top}}, \frac{C_b M_{cr1.bot}}{M_{max.bot}}\right) \quad (2)$$

where the subscripts *top* and *bot* designate the "top" and "bottom" flanges of the section, as defined in the preceding text. It should be observed that Equation 2 is based on equating $\gamma_{eLTB}\, M_{max.top}$ to $C_b M_{cr1.top}$ for the top flange and

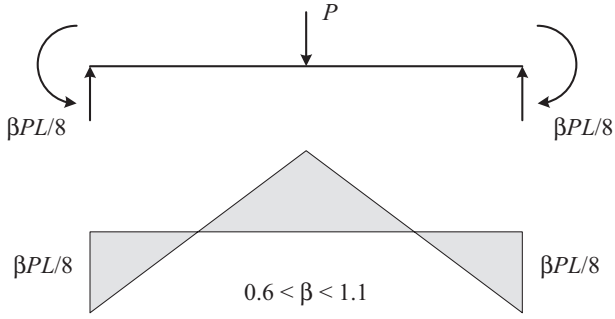

Fig. 3. Cases from Wong and Driver where the AISC C_b *equation overpredicts benchmark solutions.*

$\gamma_{eLTB} M_{max.bot}$ to $C_b M_{cr1.bot}$ for the bottom flange. For single-curvature bending, only the direction of bending causing compression in the single compression flange is considered.

In the ASC procedure, the C_b value calculated from ASC Equation C-F1-3 applies in all cases when evaluating the elastic LTB resistance corresponding to flexural compression in the "critical flange," which is defined as the flange having the largest M_{max}/M_{cr1} in Equation 2.

It can be observed that ASC Equation C-F1-3 is blind to the sign of the bending moment. The values input to ASC Equation C-F1-3 are all absolute values of the moments at the corresponding locations. In addition, the R_m factor does not include any consideration of the sign or the shape of the moment diagram along the unbraced length. As such, the ASC C_b calculation does not account for different patterns of compression and tension in the different size flanges for a general case involving moment reversal. The single ASC C_b value is applied to the two distinct member LTB resistances for uniform positive and negative bending, $M_{cr1.top}$ and $M_{cr1.bot}$. However, the C_b modifier being applied to these resistances does not account for where and to what extent the different flanges are being placed in flexural compression. As a result, the final solution for the LTB resistance has limited accounting for these effects.

Equation 1b for the R_m factor was derived considering only moment diagrams for fixed-fixed and propped cantilever members that have no lateral bracing throughout their entire span. Helwig et al. (1997) state that ASC Equation C-F1-3 is quite conservative for cases with linear moment diagrams in reverse-curvature bending and smaller values of $I_{y.opp}/I_y$. They refer to Kitipornchai et al. (1986) for more accurate C_b estimates in these situations. For linear moment diagrams, the AASHTO procedure gives accurate to moderately conservative calculations relative to the more complex equations presented by Kitipornchai et al. It is submitted that accurate solutions for near linear moment diagram cases are important to the design efficiency in many situations. This is because, when a member has at least some lateral bracing within its span, the shape of the moment diagram becomes relatively close to linear within each unbraced length. Furthermore, the moment diagrams for column members are typically close to being linear.

AASHTO Procedure

The AASHTO procedure is presented in terms of elastic flange stresses in Article 6.10.8, and in terms of moments in Article A6.3.3. For noncomposite prismatic I-section members, the stresses in a given flange are simply the moments divided by the elastic section modulus to the flange; therefore, the same result is obtained whether the demands are written as flange stresses or as moments. As such, for the purposes of this paper, the AASHTO procedure is expressed entirely in terms of member moments:

For unbraced lengths where $M_{mid}/M_2 \geq 1.0$, or when $M_2 = 0$,

$$C_b = 1.0 \tag{3}$$

Otherwise,

$$C_b = 1.75 - 1.05\frac{M_1}{M_2} + 0.3\left(\frac{M_1}{M_2}\right)^2 \leq 2.5 \tag{4}$$

where

M_{mid} = the moment at the middle of the unbraced length taken as positive when it causes compression and negative when it causes tension in the flange being considered, kip-in. (N-mm)

M_0 = the actual moment at the brace point opposite to the one corresponding to M_2, taken as positive when it causes compression and negative when it causes tension in the flange under consideration, kip-in. (N-mm)

M_1 = the equivalent moment at the brace point opposite to the one corresponding to M_2, calculated as the intercept of the most critical assumed linear moment variation passing through M_2 and either M_{mid} or M_0, whichever produces the smaller value of C_b, kip-in. (N-mm); M_1 is calculated as follows:

- When the variation in the moment along the entire unbraced length is concave in shape corresponding to the flange in compression (i.e., the stress in the flange under consideration is a smaller compressive value or a larger tensile value at the mid-length, compared to a value obtained as the average of the end moments),

  $$M_1 = M_0 \tag{5}$$

- Otherwise, the moment diagram is defined as convex in shape, and

  $$M_1 = 2M_{mid} - M_2 \geq M_0 \tag{6}$$

M_2 = the largest moment at either end of the unbraced length causing compression in the flange under consideration, taken as a positive value kip-in. (N-mm), except as noted in the following text; if the moment is zero or causes tension in the flange under consideration at both ends of the unbraced length, M_2 is taken as zero

The AASHTO method amounts to fitting a line from the maximum end moment through the mid-point of the moment diagram if the moment diagram is convex, and to fitting a line through both end points of the diagram if the diagram is concave. The actual maximum limit of 2.3 in AASHTO (2020) is increased to 2.5 in Equation 4 as discussed in the Background section of this paper.

For reverse-curvature bending cases, the AASHTO procedure applies Equations 3 through 6 separately to calculate a different C_b for each flange. Nonlinear moment diagrams are always concave on one flange and convex on the other in these cases. The corresponding elastic buckling load ratio is:

$$\gamma_{eLTB} = \min\left(\frac{C_{b.top}M_{cr1.top}}{M_{max.top}}, \frac{C_{b.bot}M_{cr1.bot}}{M_{max.bot}}\right) \quad (7)$$

For single-curvature bending, only the direction of bending causing compression in the single compression flange is considered.

If Equations 5 and 6 are substituted into Equation 4, the resulting calculation can be written more directly as:

$$C_b = 1.75 - 1.05\frac{M_0}{M_2} + 0.3\left(\frac{M_0}{M_2}\right)^2 \le 2.5 \quad (8)$$

for a concave moment diagram, and

$$C_b = 3.10 - 3.30\frac{M_{mid}}{M_2} + 1.2\left(\frac{M_{mid}}{M_2}\right)^2 \le 2.5 \quad (9)$$

for a convex moment diagram.

For reverse-curvature bending, the C_b value for the flange that governs the calculation of γ_{eLTB} in Equation 7 is considered as the "governing" C_b.

Clearly, the AASHTO procedure has a major limitation in that, when the maximum moment causing compression in the flange under consideration occurs within the unbraced length instead of at one of the ends, it simply uses $C_b = 1$. The AASHTO Commentary suggests that other methods such as the ASC procedure should be considered for the calculation of C_b in these cases.

One advantage of the AASHTO procedure is that it only requires the end moments and the moment at the middle of the unbraced length for its calculations; therefore, it may be considered as being simpler to apply. The end moments typically are readily available from a structural analysis. The quarter-point formulas require the moments at the quarter- and mid-points as well as the maximum moment within the unbraced length, requiring some additional work. However, the subsequent strength design checks also require the calculation of the maximum positive and negative moments within the unbraced length in any case; therefore, it can be argued that the quarter-point formulas are not significantly more difficult to apply.

Recommended Procedure

For singly symmetric cases, the recommended moment gradient factor calculation directly applies the quarter-point formula developed by Wong and Driver:

$$C_b = \frac{4M_{max}}{\sqrt{M_{max}^2 + 4M_A^2 + 7M_B^2 + 4M_C^2}}$$

(AISC *Spec*. Comm. Eq. C-F1-2b)

However, for singly symmetric sections subjected to reverse-curvature bending, the Wong and Driver equation is modified to the following form:

$$C_b = \frac{4\left(\frac{M}{M_{cr1}}\right)_{max}}{\sqrt{\left(\frac{M}{M_{cr1}}\right)_{max}^2 + 4\left(\frac{M}{M_{cr1}}\right)_A^2 + 7\left(\frac{M}{M_{cr1}}\right)_B^2 + 4\left(\frac{M}{M_{cr1}}\right)_C^2}} \quad (10)$$

where

M_{cr1} = base elastic critical moment corresponding to the cross section at the location under consideration (i.e., location A, B, C, or the location of the maximum M/M_{cr1}), based on uniform bending causing moment producing compression in the flange subjected to compression at this location, kip-in. (N-mm)

In the recommended procedure, the elastic buckling load ratio is estimated simply as:

$$\gamma_{eLTB} = \frac{C_b}{\left(\frac{M}{M_{cr1}}\right)_{max}} \quad (11)$$

where C_b is calculated from ASC Equation C-F1-2b for single-curvature bending and from Equation 10 for reverse-curvature bending. It should be observed that Equation 11 is derived by equating $\gamma_{eLTB}M$ to C_bM_{cr1} at the location where M/M_{cr1} is maximum. For single-curvature bending, only the direction of bending causing compression in the single compression flange is considered. For reverse-curvature bending, $(M/M_{cr1})_{max}$ is taken as the largest value of $M/M_{cr1.top}$ from all the cross sections where the top flange is in compression, and $M/M_{cr1.bot}$ from all the cross sections where the bottom flange is in compression, inclusive. This is equivalent to the use of the ASC-based Equation 2, but with a more accurate C_b.

For reverse-curvature bending cases, Equation 10 incorporates essential information about the shape of the moment diagram and the demands versus a corresponding base capacity in uniform bending at the different sampling points throughout the unbraced length. The simplicity of the C_b calculation is improved relative to the current methods, because $M_{cr1.top}$ and $M_{cr1.bot}$ need to be calculated in all the procedures, and the calculations of R_m in the ASC procedure and multiple C_b values in the AASHTO procedure are avoided.

A major advantage of the recommended method is that it provides comparable or greater accuracy in capturing the results from benchmark C_b calculations in all cases, compared to the ASC and AASHTO approaches, while maintaining essentially the same degree of simplicity as these procedures. The recommended method solves the problem of sharp discontinuities in the ASC and AASHTO C_b estimates, where the ASC solution gives either significantly conservative or unconservative results, and where the AASHTO solution gives significantly conservative results. These attributes are investigated in detail in the following sections of the paper.

Calculation of Benchmark C_b Values

The most rigorous method of determining the elastic LTB resistance is via an elastic buckling analysis based on the same thin-walled open-section (TWOS) beam theory that the AISC *Specification* flexural resistance equations are based upon. This research employs a general-purpose TWOS frame finite element developed by Jeong (2014) to generate a large dataset of converged benchmark solutions. The torsionally and flexurally simply supported unbraced lengths considered in this study are analyzed using 32 elements, although eight elements within the unbraced length are sufficient to obtain converged results within 1% of the analytical solution in all cases. The reader is referred to Jeong (2014) and White et al. (2021) for various validation studies demonstrating the efficacy of this finite element.

The first step of the computational solution is to determine the first (lowest) eigenvalue from an elastic linear buckling analysis conducted for a given finite element model of a selected physical beam. This eigenvalue is precisely the benchmark γ_{eLTB}. Given this eigenvalue, the moment gradient factor for the top flange, when the top flange is subjected to flexural compression, is:

$$C_{b.top} = \frac{\gamma_{eLTB} M_{max.top}}{M_{cr1.top}} \tag{12}$$

and the moment gradient factor for the bottom flange, when the bottom flange is subjected to flexural compression, is:

$$C_{b.bot} = \frac{\gamma_{eLTB} M_{max.bot}}{M_{cr1.bot}} \tag{13}$$

The governing C_b is the one corresponding to the critical flange, which is defined as the flange that has the largest M_{max}/M_{cr1}. This converged numerically generated value of C_b may be taken as the "exact" moment gradient factor corresponding to flexural compression in the critical flange.

PARAMETRIC STUDY DESIGN—LOADING CASES

As noted in the Introduction and Background, design expressions for C_b should be accurate for near-linear moment diagrams as well as for highly nonlinear moment diagram cases. This objective is addressed in this study by:

1. Directly evaluating the performance of the different methods for a complete range of linear moment diagram cases.
2. Varying the "nonlinearity" of the moment diagrams as a direct function of the ratio of the moments due to the transverse loads to the maximum end moments on the unbraced lengths.

Figure 4 shows the parametric variations selected for linear moment diagram cases in this study. In these cases, the "right-hand" end of the unbraced length is subjected to the moment M_R and the "left-hand" end is subjected to the moment $M_L = \alpha M_R$. The reader should note that "left-" and "right-hand" end are actually immaterial in these studies, because if the reader walks around to the opposite side of the member being considered and views the member from there, the "left" end becomes the "right" and vice versa. These moments are equilibrated by the shear forces applied at the ends of the unbraced length, and it is assumed that any other loadings within the unbraced length are negligible. For doubly symmetric members, one need only consider values of α between –1.0 and 1.0, as considered previously in Figures 1 and 2. However, for singly symmetric members, it is important to consider reverse-curvature bending cases in which the inflection point is located at various locations throughout the unbraced length; furthermore, both sections with a larger as well as a smaller "top" flange should be addressed. The variation in the relative flange sizes is captured in this study by the monosymmetry parameter:

$$\rho = \frac{I_{y.top}}{I_y} \cong \frac{1}{1 + \dfrac{I_{y.bot}}{I_{y.top}}} \tag{14}$$

where

I_y = weak-axis moment of inertia of the entire cross section, in.^{4} (mm^4)

$I_{y.bot}$ = moment of inertia of the bottom flange about an axis in the plane of the web, in.^{4} (mm^4)

$I_{y.top}$ = moment of inertia of the top flange about an axis in the plane of the web, in.^{4} (mm^4)

The maximum and minimum limits on ρ of 0.9 and 0.1 employed in this work are the same as in the AISC *Specification* Equation F13-2. Values of ρ = 0.1, 0.3, 0.5, 0.7, and 0.9 are considered.

Regarding practical cases involving "nonlinear" moment diagrams, two types of transverse loading are considered within the unbraced lengths in this research:

1. A concentrated load, *P*, applied at the web mid-height and middle of the unbraced length.
2. A uniformly distributed load, *w*, applied throughout the unbraced length.

These loadings encompass all of the loading cases considered by Helwig et al. (1997) as well as the majority of the loading cases studied by Wong and Driver. However, in this research, loadings that involve a small deviation from the basic linear moment diagrams are emphasized in addition to loadings that are more akin to transversely loaded members that do not have any bracing within their entire span. This is accomplished by varying two parameters,

$$\alpha = \frac{M_L}{M_R} \tag{15}$$

and

$$\zeta = \frac{M_{ss}}{M_R} \tag{16}$$

where M_{ss} is the maximum "simply supported" moment associated with a given transverse loading, located at the middle of the unbraced length. For the first transverse loading case,

$$M_{ss} = \frac{PL_b}{4} \tag{17}$$

and for the second loading case,

$$M_{ss} = \frac{wL_b^2}{8} \tag{18}$$

The following values of α and ξ are considered for the nonlinear moment diagram cases:

- α values of + 1.0, + 0.5, 0, −0.5, and −1.0.
- ξ values ranging from −2.0 to + 2.0 for each of these α values, with $\Delta\xi$ taken as 0.1.

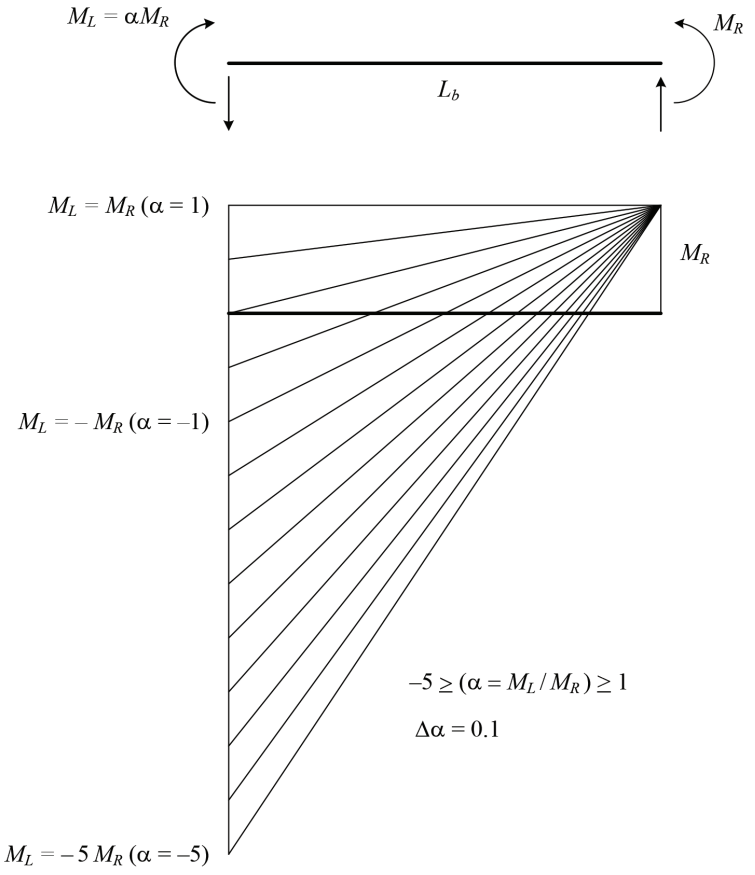

Fig. 4. Linear moment diagrams considered in this study.

These combinations of α and ξ produce the moment diagrams illustrated in Figure 5. The "base" linear moment diagrams corresponding to $\xi = 0$ are indicated by the dashed lines in each of the plots, and the moment diagrams corresponding to nonzero transverse loads for $\xi = 2.0$, 1.0, –1.0, and –2.0, applied in addition to the end moments, are indicated by the solid lines.

Simply supported unbraced lengths with zero end moments are not considered in this study. The specified loadings produce a range of cases combined with applied end moments that are considered sufficient to validate the application of the C_b design expressions, which were developed originally for doubly symmetric I-section unbraced lengths, to singly symmetric I-section members subjected to single-curvature bending. Given the validations shown here, the specific single-curvature bending cases investigated in Helwig et al. (1997) and the wider range of single-curvature bending cases investigated by Wong and Driver are considered as further validation of use of the C_b design expressions for doubly and singly symmetric members subjected to single-curvature bending. The current study focuses on cases where there is always a nonzero moment of some sign at one or both ends of the unbraced length.

In addition to simply supported unbraced lengths, Helwig et al. (1997) considered fixed-fixed and propped cantilever beams with uniformly distributed transverse load as well as a single concentrated transverse load at their mid-span. These loading cases correspond to the following specific (α, ξ) combinations:

- For the transverse concentrated load cases, (α, ξ) = (1.0, –2.0) for the fixed-fixed beams and (0.0, –1.33) for the propped cantilever beams.
- For the uniformly distributed transverse load cases, (α, ξ) = (1.0, –1.5) for the fixed-fixed beams and (0,0, –1.0) for the propped cantilever beams.

Wong and Driver considered a wider range of loadings, but only for doubly symmetric beams, and with an emphasis on (1) beams with no bracing within their entire span and (2) loadings in which the end moments are small compared to the simply supported moments. In addition to their cases that fit within the range of the loadings studied in this work, they studied:

- Simply supported beams with a concentrated transverse load applied at a variable location between the beam end and the mid-span (referred to as their loading type 6).
- Simply supported beams with two concentrated transverse loads applied at a variable equal distance from the end supports (referred to as their loading type 7).
- Concentrated transverse loads applied at the third points of the unbraced length, combined with equal and opposite variable end moments (referred to as their loading type 11).
- Concentrated transverse loads applied at the third points of the unbraced length, combined with zero moment at one end and a variable applied moment at the opposite end of the unbraced length (referred to as their loading type 12).

The authors submit that the two transverse loading cases combined with the α and ξ values considered in this study, plus the additional cases from Wong and Driver, gives a comprehensive assessment of the behavior of the different C_b design expressions for all types of loadings on both doubly and singly symmetric I-section members. The loadings considered in the current study produce practical moment diagrams for cases where there are one or more braced points within the span as well as for cases in which there is no bracing within the entire span.

Wong and Driver also considered several loading cases in which concentrated moments are applied to the member within the unbraced length. They demonstrated that none of the available C_b equations are sufficient to evaluate the LTB resistance for beams subjected to these types of loadings. These types of loadings are considered as appropriate candidates for the direct application of computational tools such as SABRE2 (White et al., 2021).

As noted previously, Helwig et al. (1997) showed that the web mid-height, rather than the shear center, is the proper transverse load position for development of base C_b equations that neglect load height. For instance, members with a very large "top" flange have a shear center close to the top flange. There is a definite destabilizing effect of downward transverse loads applied "high" on the cross section—say, at this shear center location—and a stabilizing effect of downward transverse loads applied "low" in the cross section (but relative to the web mid-height, not relative to the shear center). Helwig et al. found that if the load position is defined at the web mid-height rather than the shear center, the degree of monosymmetry does not affect the C_b values. In addition, they found that the base C_b values derived for doubly symmetric members work well for single-curvature bending cases. Furthermore, it can be stated that:

- For cases where significant end moments are applied to the unbraced length, particularly when these moments cause single-curvature bending, the influence of the height of the applied loads within the unbraced length tends to be relatively small. Simply stated, this is because the portion of the moment coming from the transverse loading is small in these cases.
- In addition, regarding load-height effects, it should be understood that in many situations involving transverse loads, the application of the load itself involves "tipping

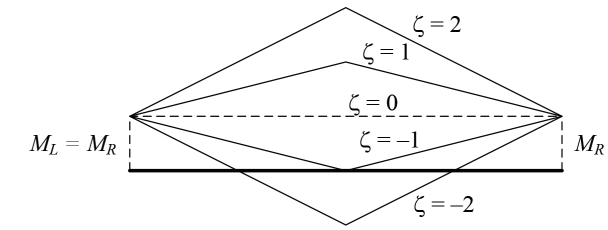

(a) $\alpha = 1.0$, CL*

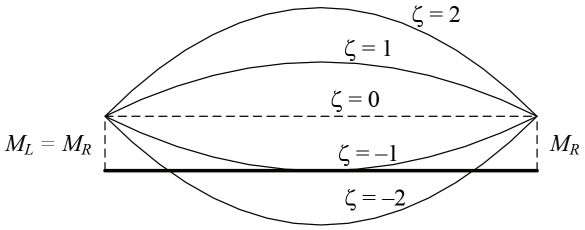

(f) $\alpha = 1.0$, UDL*

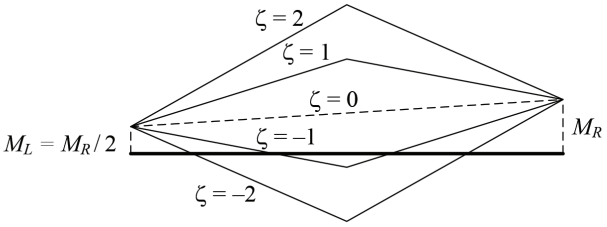

(b) $\alpha = 0.5$, CL

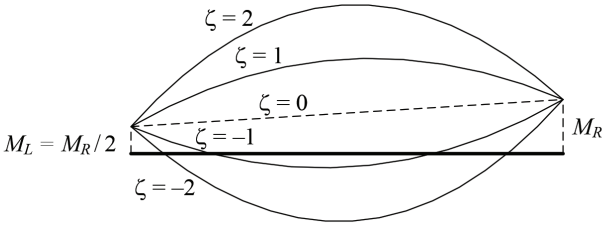

(g) $\alpha = 0.5$, UDL

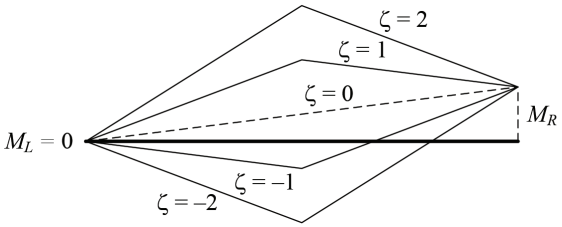

(c) $\alpha = 0.0$, CL

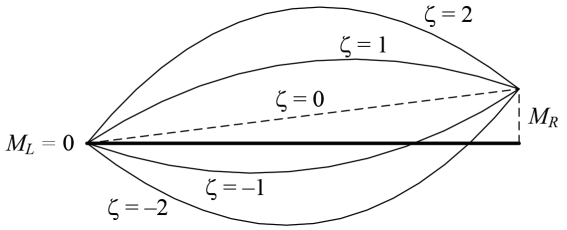

(h) $\alpha = 0.0$, UDL

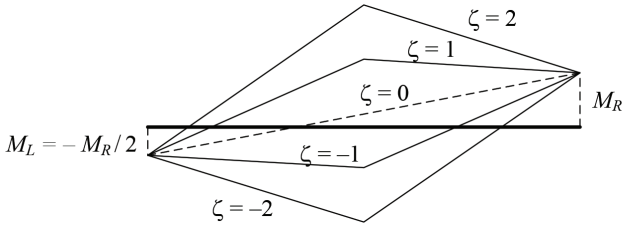

(d) $\alpha = -0.5$, CL

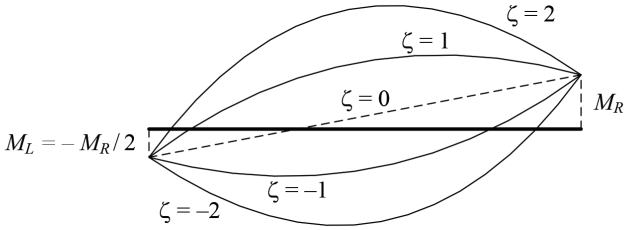

(i) $\alpha = -0.5$, UDL

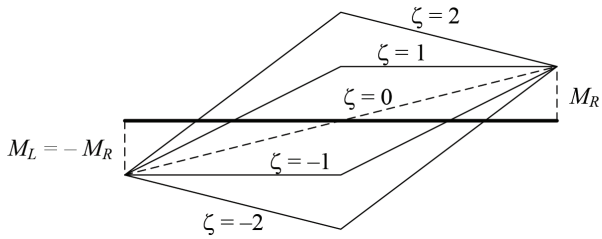

(e) $\alpha = -1.0$, CL

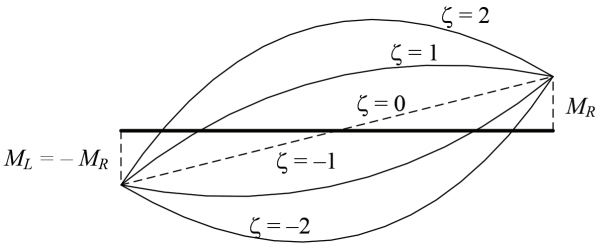

(j) $\alpha = -1.0$, UDL

Fig. 5. Nonlinear moment diagrams considered in this study (CL = concentrated load; UDL = uniformly distributed load).

restraint" from the loading mechanism (e.g., from decking), which tends to nullify the influence of any load height. Helwig et al. provide a thorough discussion of this behavioral attribute.

All of the solutions generated in this research are based on loads applied at the web mid-height.

PARAMETRIC STUDY—MEMBER GEOMETRIES

The I-section geometries for the current study are generated from the base doubly symmetric cross section shown in Figure 6. This cross section is similar to the base doubly symmetric girder cross section employed by Helwig et al. (1997). The web of the base cross section considered in this research is 60 in. × 0.5 in., which qualifies as a noncompact web but has a slenderness close to the AISC *Specification* noncompact web limit of $5.7\sqrt{E/F_y}$ = 137 for F_y = 50 ksi. The section employed by Helwig et al. had h_o (the distance between the flange centroids) = 60 in. and a web thickness of t_w = 0.736 in., which satisfies the AISC *Specification* compact-web requirements for the base cross section. The flanges of the base cross section considered in this research are 18 in. × 1.5 in., which satisfy the compact flange requirements. The flanges considered by Helwig et al. were 12 in. × 1 in. The larger base 18 in. × 1.5 in. flanges employed in this study allow for the variation in the ρ factor (Equation 14), by reducing the flange widths, without producing excessively narrow flanges relative to the section depth.

As stated at the beginning of the discussion of the loading cases for the parametric study, ρ factors of 0.1, 0.3, 0.5 (the base doubly symmetric I-section), 0.7, and 0.9 are considered in this work. In this study, the flange widths

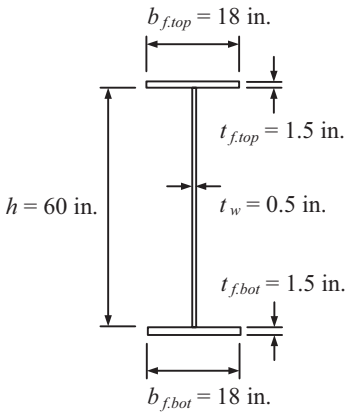

Fig. 6. Base doubly symmetric I-section employed in the current studies.

are reduced without changing the flange thickness to produce the targeted singly symmetric I-sections. For ρ = 0.1 and 0.3, the top flange width is reduced to $b_{f.top}$ = 8.65 and 13.57 in., respectively. Similarly, for ρ = 0.7 and 0.9, the bottom flange width is reduced to $b_{f.bot}$ = 13.57 and 8.65 in., respectively. The overall maximum web depth to flange width, h/b_f is therefore 60/8.65 = 6.94 in this study, which is allowed by the AISC *Specification* (with a reduced girder tension field action web shear resistance), and is only slightly larger than the largest h/b_f allowed by AASHTO for bridge girders. Helwig et al. appear to reduce the flange widths and thicknesses proportionally to vary ρ in their research. This requires a minimum flange width of 6.94 in. for their girders, giving a maximum h/b_f of 8.53.

In addition to the effect of the monosymmetry factor, the LTB resistance of both doubly and singly symmetric I-section members is influenced significantly by the nondimensional factor

$$W = \frac{\pi}{L_b}\sqrt{\frac{EC_w}{GJ}} \tag{19}$$

where C_w and J are the warping and St. Venant torsion constants of the cross section, respectively. The factor W is a measure of the contribution of the warping rigidity relative to the St. Venant torsional rigidity to the elastic LTB resistance.

The elastic LTB moment of a singly symmetric I-section beam may be expressed analytically as:

$$M_{cr} = C_b\frac{\pi^2 EI_y}{L_b^2}\left[\frac{\beta_x}{2} + \sqrt{\left(\frac{\beta_x}{2}\right)^2 + \frac{C_w}{I_y}\left(1+\frac{1}{W^2}\right)}\right] \tag{20}$$

where the coefficient of monosymmetry, β_x, may be approximated by the equation

$$\beta_x = 0.9h_o\rho_f\left(\frac{I_{yc}}{I_{yt}} - 1\right) \tag{21}$$

(Ziemian, 2010). An exact expression for β_x consistent with the thin-walled open-section FEA model employed in this research is presented by Ziemian. Equation 20 for M_{cr} is employed with the exact calculation of β_x in the evaluation of all the C_b estimates considered in this paper.

In the previous equations, h_o is the distance between flange centroids, ρ_f is defined as:

$$\rho_f = \frac{1}{1+\frac{I_{yc}}{I_{yt}}} \tag{22}$$

and I_{yc} and I_{yt} are the moments of inertia of the compression and tension flanges, respectively, about an axis in the plane of the web. In addition, the warping constant may be written as:

Table 1. Range of *W* Values Considered in the Current Parametric Study				
L_b/h_o	*J* (in.^{4})	*W* (ρ = 0.1 & 0.9)	*W* (ρ = 0.3 & 0.7)	*W* (ρ = 0.5)
10	0.0	∞	∞	∞
5	> 0	1.57	2.50	3.03
10	> 0	0.786	1.25	1.51
20	> 0	0.393	0.626	0.758
30	> 0	0.262	0.417	0.504

$$C_w = h_o^2 I_{yc} \rho_f \tag{23}$$

Therefore, the different terms in Equation 20 may be approximated as follows:

$$\beta_x = 0.9 h_o \frac{\frac{I_{yc}}{I_{yt}} - 1}{\frac{I_{yc}}{I_{yt}} + 1} \tag{24}$$

$$W = \frac{\pi}{L_b}\sqrt{\frac{EC_w}{GJ}} \tag{25}$$

$$= \frac{\pi}{(L_b/h_o)}\sqrt{\frac{EI_{yc}\rho_f}{GJ}}$$

$$= \frac{\pi}{(L_b/h_o)}\sqrt{\frac{E}{G}\frac{1}{J}\frac{I_{yc}I_{yt}}{I_{yc}+I_{yt}}}$$

and

$$\frac{C_w}{I_y} = \frac{h_o^2 I_{yc}}{\frac{I_{yc}}{I_{yt}}+1}\frac{1}{I_{yc}+I_{yt}} = \frac{h_o^2 I_{yc} I_{yt}}{(I_{yc}+I_{yt})^2} = \frac{h_o^2}{\left(\frac{I_{yc}}{I_{yt}}+1\right)\left(\frac{I_{yt}}{I_{yc}}+1\right)} \tag{26}$$

Considering these equations, it can be observed that for a given singly symmetric cross section, there is one *J* value, one C_w value, one C_w/I_y value, and one *W* value irrespective of which flange is in compression. That is, the selected singly symmetric cross sections with ρ = 0.1 and 0.9 have the same *J*, C_w, C_w/I_y, and *W* values. Also, the singly symmetric cross sections with ρ = 0.3 and 0.7 have the same *J*, C_w, C_w/I_y, and *W* values, but these are different from the values for ρ = 0.1 and 0.9. The coefficient of monosymmetry, β_x, is influenced by which flange is in flexural compression. Furthermore, it can be observed in general that the nondimensional parameters I_{yc}/I_{yt} and *W* have a substantial influence on the elastic LTB resistance. By inference, it can be expected that these parameters may also have an impact on the moment gradient factor, C_b.

Considering the behavior associated with Equations 20 through 26, one can conclude that *W* needs to be varied over a comprehensive range, in addition to the variation of ρ, to fully evaluate the ability of design expressions to capture benchmark C_b values obtained from converged numerical solutions. In the current study, this is achieved by varying L_b/h_o as well as by varying the St. Venant torsion constant *J* via the selected cross-section dimensional variations.

The values of L_b/h_o considered in this research are 5, 10, 20, and 30. Further, one additional suite of parametric study beams is considered with L_b/h_o = 10 and with *J* taken equal to zero. For *J* = 0, the thin-walled open-section beam theory solution for the compression flange stress at elastic LTB is essentially independent of L_b/h_o. The assumption of *J* = 0, which is applied in the AISC and AASTHO *Specifications* when the web classifies as slender, effectively gives *W* = ∞, while L_b/h_o = 30 with a finite *J* (calculated from AASHTO Equation A6.3.3-9 in this work) gives representative practical minimum values for *W*. The *W* values considered in the current study, as a function of L_b/h_o and finite or zero *J*, are summarized in Table 1.

RESULTS

Figures 7 through 12 present sample results from this study as plots of the benchmark and estimated C_b values versus the independent variables ρ, α, and ξ, all for members with L_b/h_o = 10. The unbraced length to depth ratio L_b/h_o = 10 is selected for the plots in these figures because this is a representative intermediate value of L_b/h_o.

Figure 7 summarizes the results for the linear moment cases (ξ = 0). This is followed by Figures 8 through 12, which summarize the results for nonlinear moment cases with a uniformly distributed transverse load. Slein et al. (2021) show plots that parallel Figures 8 through 12 for nonlinear moment cases involving members subjected to a transverse concentrated load at the middle of the unbraced length. Each of the figures are arranged into five plots to convey the physical behavior, and the predictions of this behavior by the C_b design expressions, for different ρ, α, and ξ values.

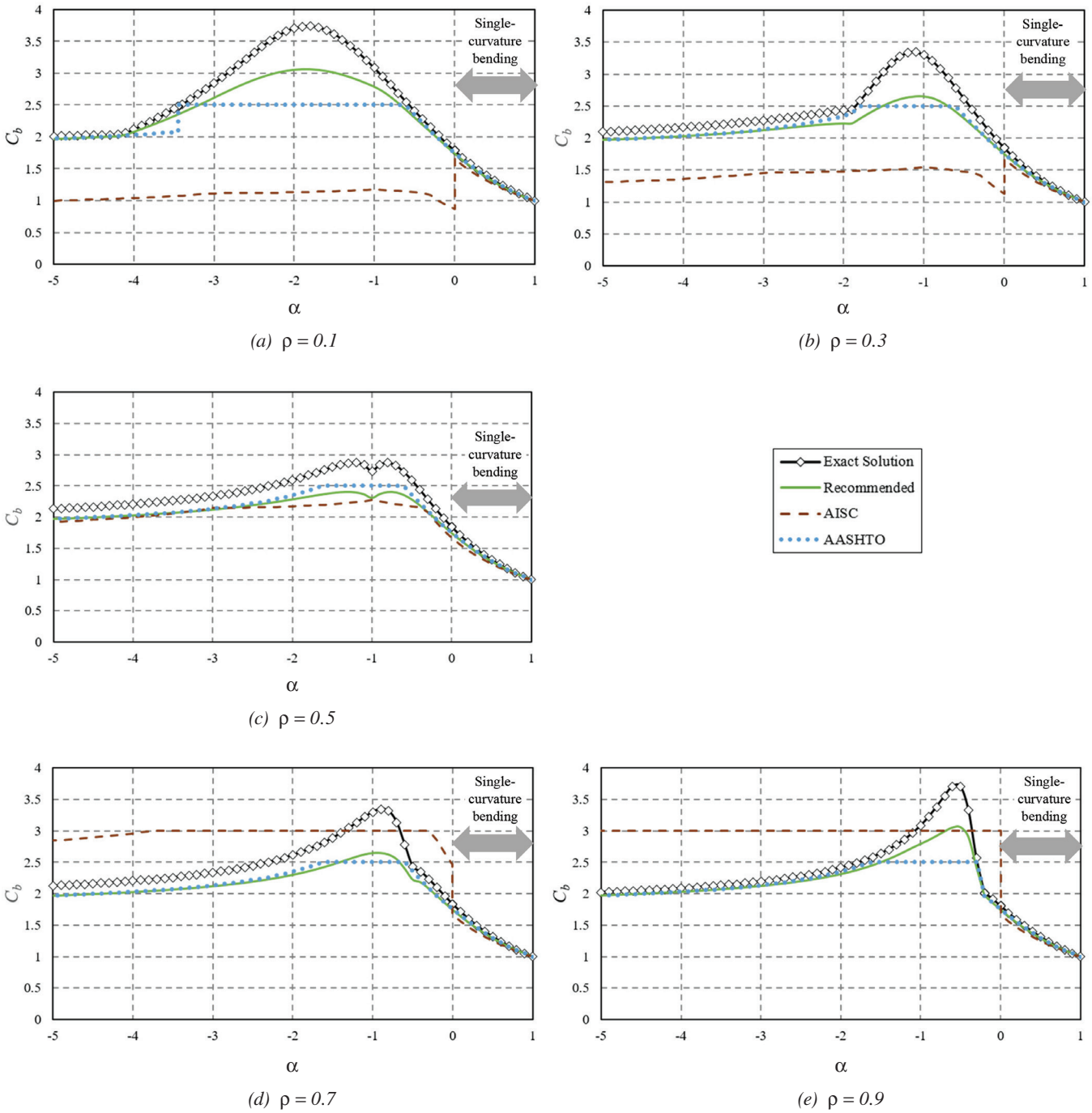

(a) $\rho = 0.1$ *(b)* $\rho = 0.3$

(c) $\rho = 0.5$

(d) $\rho = 0.7$ *(e)* $\rho = 0.9$

Fig. 7. Governing C_b *values for linear moment cases* ($\xi = 0.0$), $L_b/h_o = 10$.

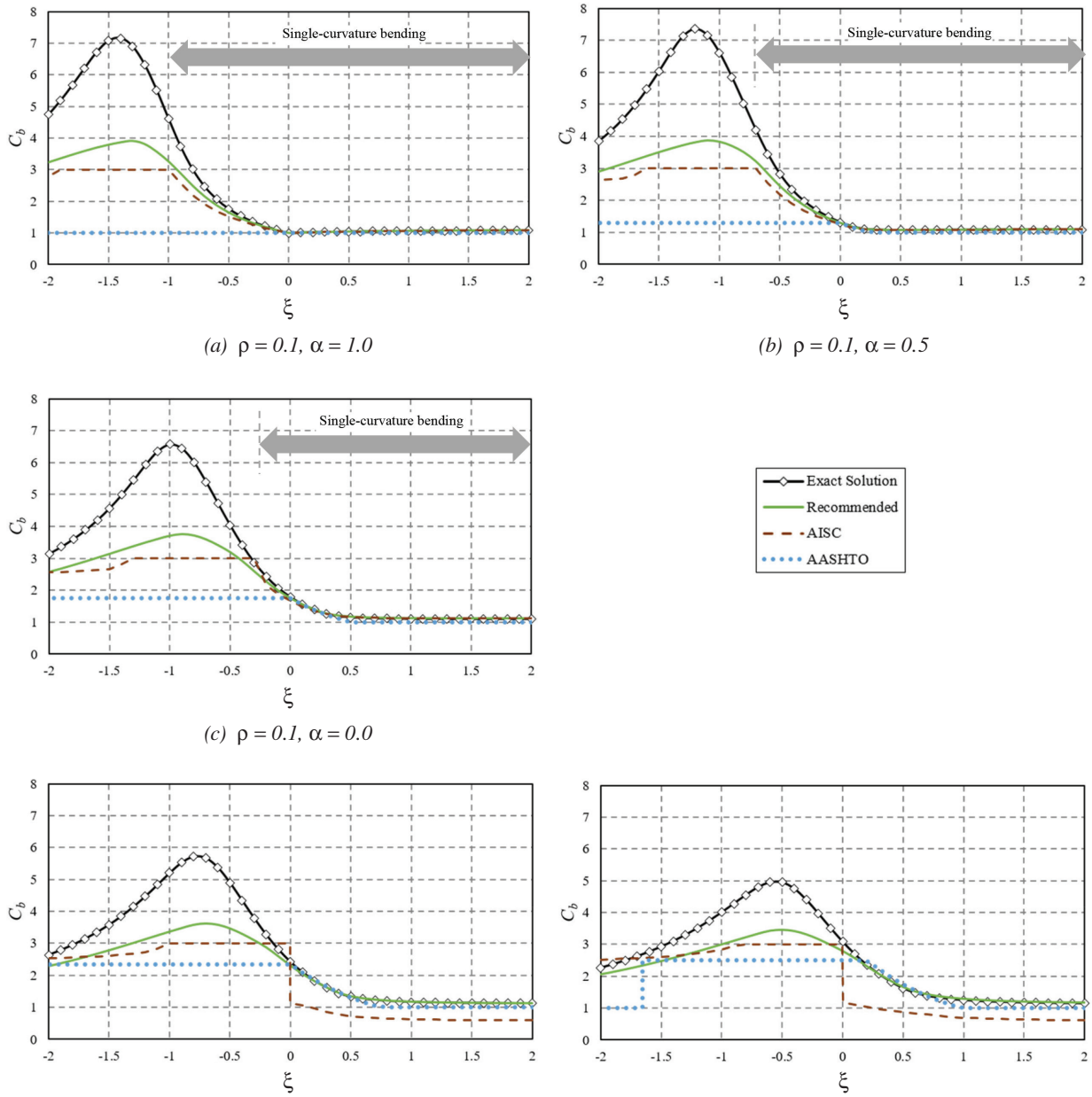

(a) $\rho = 0.1, \alpha = 1.0$ *(b)* $\rho = 0.1, \alpha = 0.5$

(c) $\rho = 0.1, \alpha = 0.0$

(d) $\rho = 0.1, \alpha = -0.5$ *(e)* $\rho = 0.1, \alpha = -1.0$

Fig. 8. Governing C_b *values for members with* $\rho = 0.1$ *and* $L_b/h_o = 10$*, subjected to a uniformly distributed transverse load:* $\alpha = 1.0, 0.5, 0.0, -0.5,$ *and* -1.0*;* ξ *ranging from* -2.0 *to* 2.0*.*

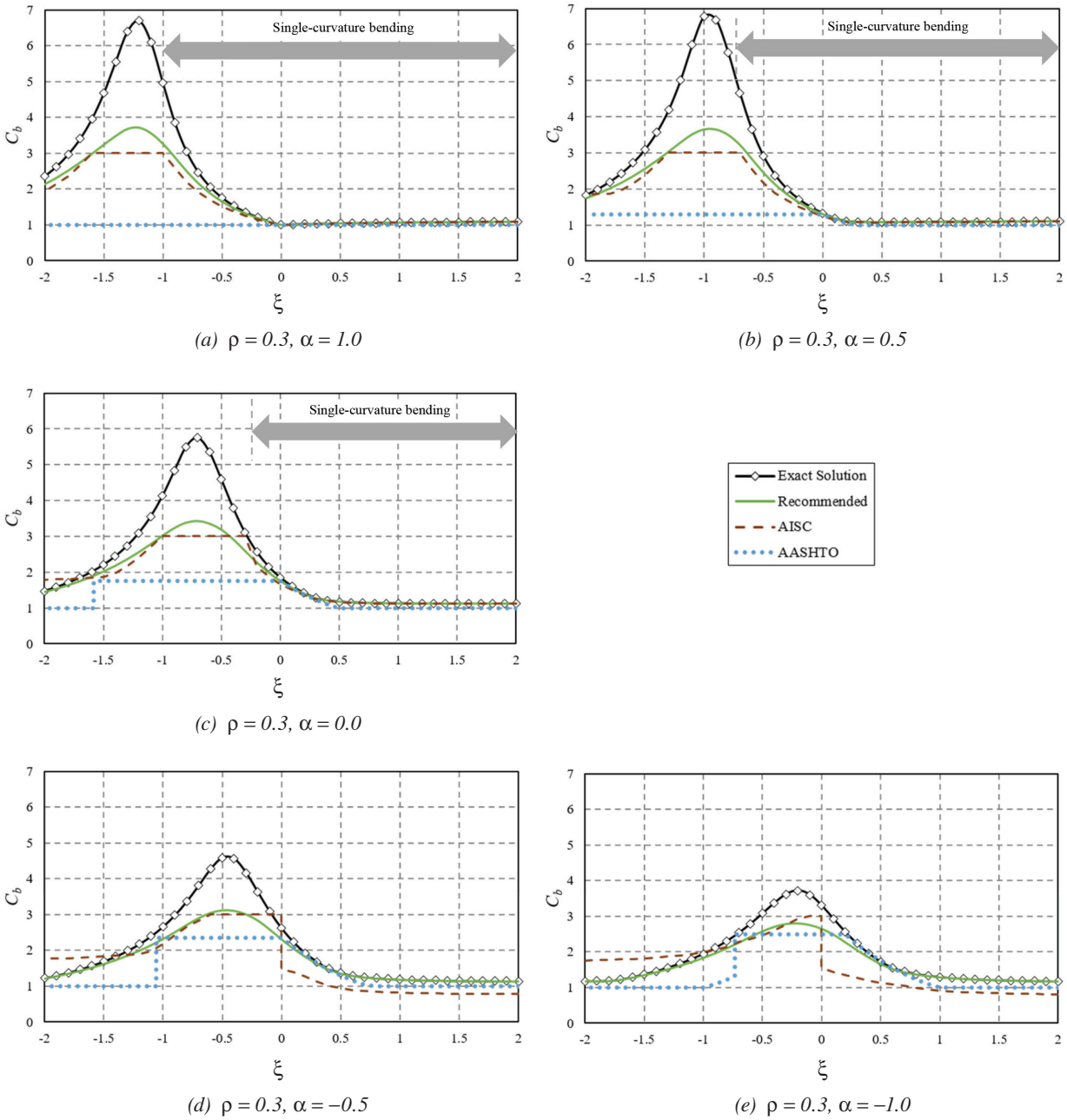

(a) $\rho = 0.3, \alpha = 1.0$

(b) $\rho = 0.3, \alpha = 0.5$

(c) $\rho = 0.3, \alpha = 0.0$

(d) $\rho = 0.3, \alpha = -0.5$

(e) $\rho = 0.3, \alpha = -1.0$

Fig. 9. Governing C_b *values for members with* $\rho = 0.3$ *and* $L_b/h_o = 10$*, subjected to a uniformly distributed transverse load:* $\alpha = 1.0, 0.5, 0.0, -0.5$*, and* -1.0*;* ξ *ranging from* -2.0 *to* 2.0*.*

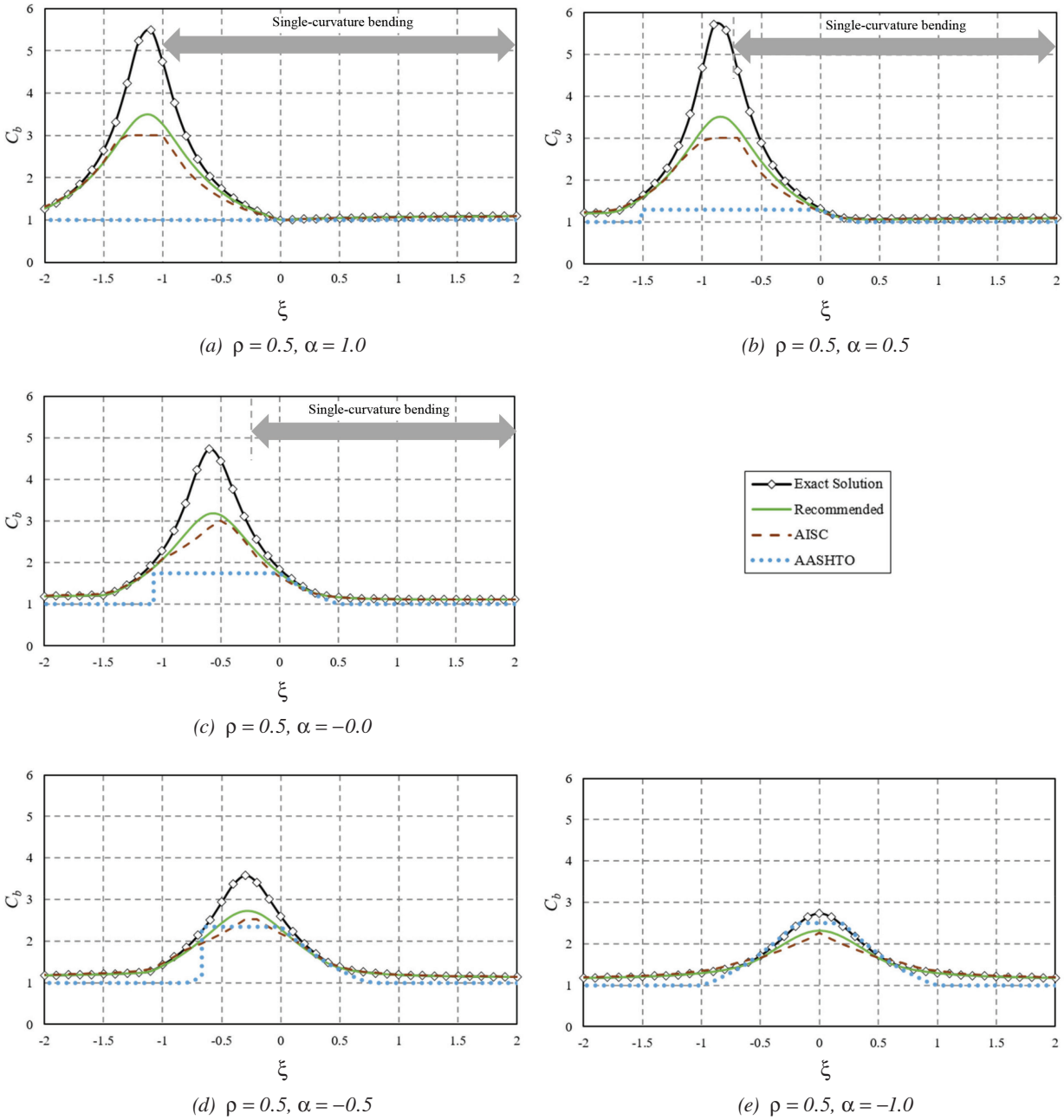

(a) $\rho = 0.5, \alpha = 1.0$ *(b)* $\rho = 0.5, \alpha = 0.5$

(c) $\rho = 0.5, \alpha = -0.0$

(d) $\rho = 0.5, \alpha = -0.5$ *(e)* $\rho = 0.5, \alpha = -1.0$

Fig. 10. Governing C_b *values for members with* $\rho = 0.5$ *and* $L_b/h_o = 10$*, subjected to a uniformly distributed transverse load:* $\alpha = 1.0, 0.5, 0.0, -0.5,$ *and* -1.0*;* ξ *ranging from* -2.0 *to* 2.0*.*

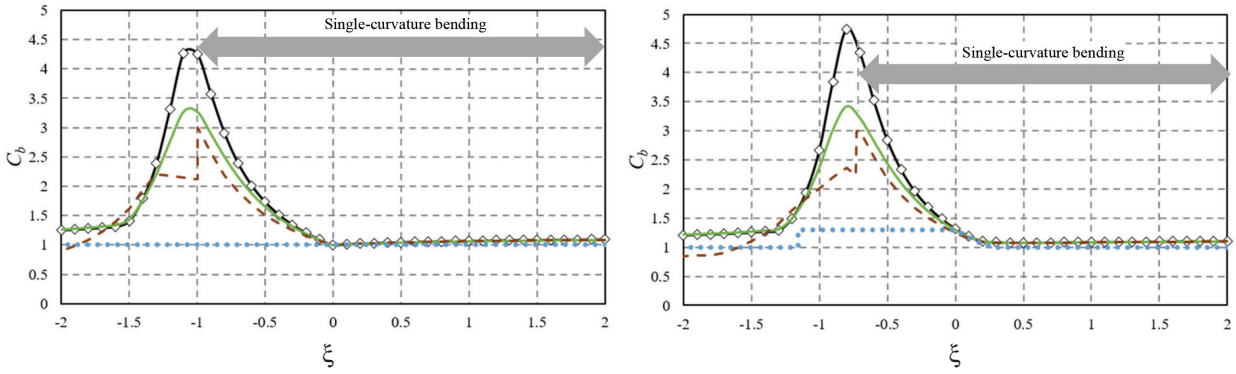

(a) $\rho = 0.7, \alpha = 1.0$

(b) $\rho = 0.7, \alpha = 0.5$

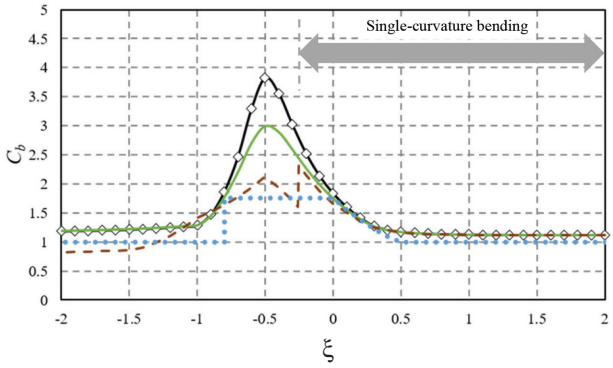

(c) $\rho = 0.7, \alpha = 0.0$

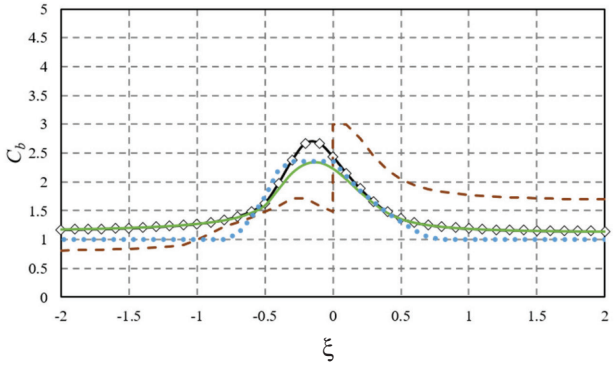

(d) $\rho = 0.7, \alpha = -0.5$

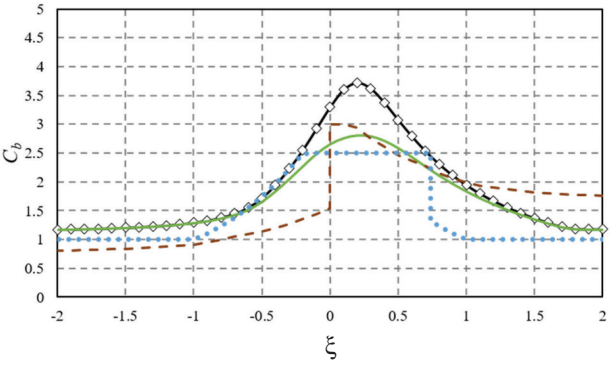

(e) $\rho = 0.7, \alpha = -1.0$

Fig. 11. Governing C_b *values for members with* $\rho = 0.7$ *and* $L_b/h_o = 10$*, subjected to a uniformly distributed transverse load:* $\alpha = 1.0, 0.5, 0.0, -0.5,$ *and* -1.0*;* ξ *ranging from* -2.0 *to* 2.0*.*

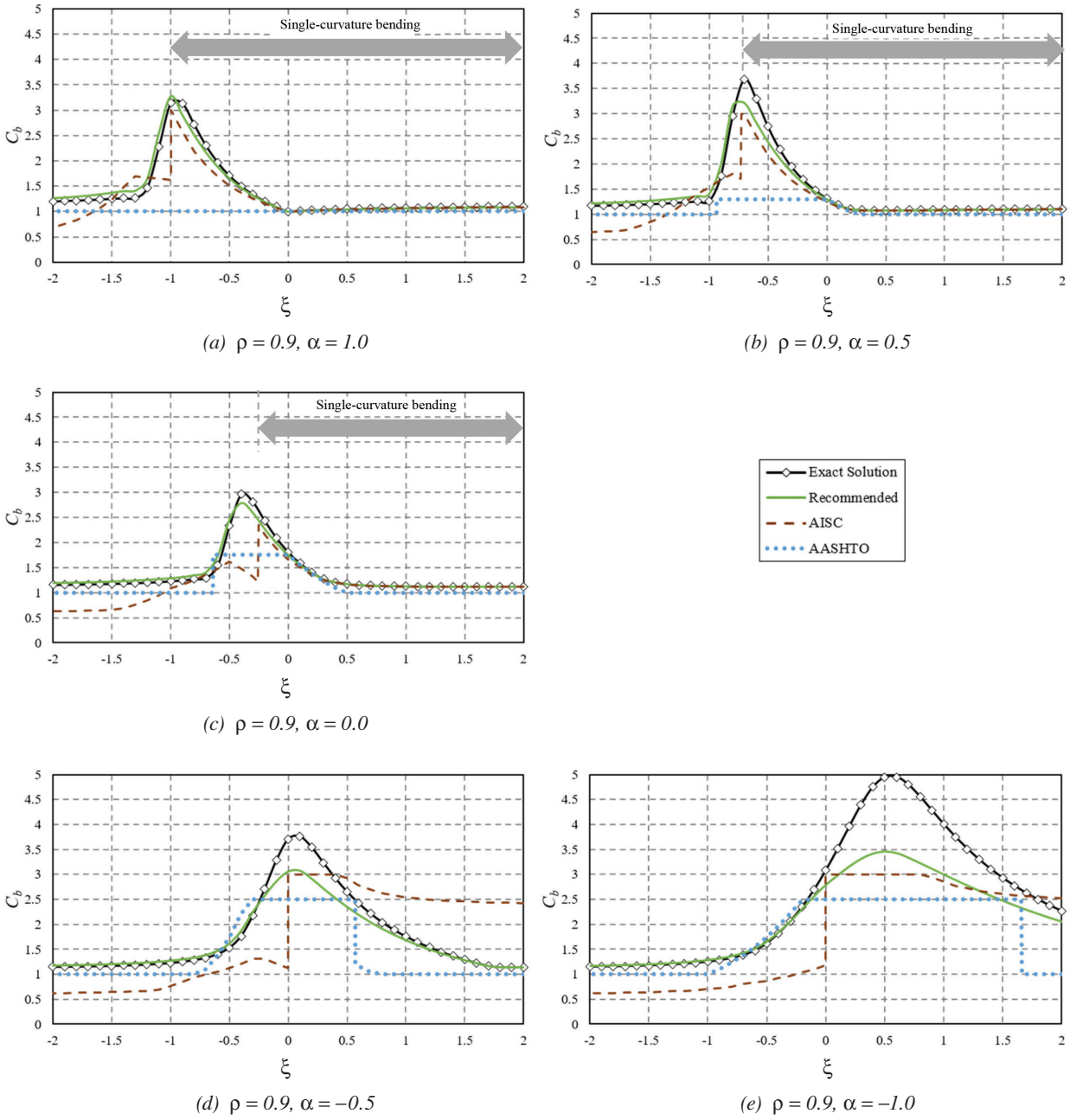

(a) $\rho = 0.9, \alpha = 1.0$ *(b)* $\rho = 0.9, \alpha = 0.5$

(c) $\rho = 0.9, \alpha = 0.0$

(d) $\rho = 0.9, \alpha = -0.5$ *(e)* $\rho = 0.9, \alpha = -1.0$

Fig. 12. Governing C_b *values for members with* $\rho = 0.9$ *and* $L_b/h_o = 10$*, subjected to a uniformly distributed transverse load:* $\alpha = 1.0, 0.5, 0.0, -0.5,$ *and* -1.0*;* ξ *ranging from* -2.0 *to* 2.0*.*

Table 2. $C_{b\ exact}/C_b$ Statistics, Linear Moment Cases, All Sections and All Values of W				
Value	**Recommended**	**ASC**	**AASHTO**	**Recommended (ASC)**
Max	1.70	5.16	2.33	1.84
Mean	1.10	1.38	1.12	1.13
Min	0.920	0.608	0.892	0.930
COV	0.104	0.569	0.180	0.112

Table 3. $C_{b\ exact}/C_b$ Statistics, Nonlinear Moment Cases—Uniformly Distributed Transverse Load and Concentrated Transverse Load at the Middle of the Unbraced Length, All Sections and All Values of W				
Value	**Recommended**	**ASC**	**AASHTO**	**Recommended (ASC)**
Max	3.26	5.13	12.43	3.01
Mean	1.11	1.24	1.55	1.11
Min	0.769	0.454	0.722	0.666
COV	0.191	0.344	0.577	0.204

In Figure 7, each of the five plots corresponds to a different ρ value, ρ = 0.1, 0.3, 0.5, 0.7, and 0.9. Values of ρ less than 0.5 correspond to a smaller "top" flange, values of ρ greater than 0.5 correspond to a larger "top" flange, and ρ = 0.5 corresponds to doubly symmetric cross sections. The horizontal axis in each of these plots corresponds to the variation in α from −5.0 to 1.0 as illustrated in Figure 4. Values of α ranging from 0.0 to 1.0 correspond to single-curvature bending. This attribute is highlighted by the annotation in the upper-right corner of the plots.

Each of Figures 8 through 12 corresponds to a specific ρ value (i.e., ρ = 0.1, 0.3, 0.5, 0.7, or 0.9). The five plots in each of these figures correspond to different end moment ratios (α) (i.e., α = 1.0, 0.5, 0.0, −0.5, and −1.0). The ratio of the simple-span moment to the maximum end moment, ξ, is varied from −2.0 to 2.0 on the horizontal axis of these plots. The moment diagrams produced by these ranges of α and ξ are illustrated in Figure 5.

For the members subjected to uniformly distributed transverse load (Figures 8 through 12), the following cases correspond to single-curvature bending:

- For α = 1.0, $\xi \geq -1.0$
- For α = 0.5, $\xi \geq -0.729$
- For α = 0.0, $\xi \geq -0.25$

These cases are highlighted by the annotation in the upper-right corner of the plots, where applicable. All of the other α and ξ values correspond to reverse-curvature bending. All the cases in Figures 8 to 12 parts (d) and (e), corresponding to $\alpha = -0.5$ and −1.0, involve reverse-curvature bending.

Figures 13 and 14 show arrays of boxplots for the ratio of the benchmark C_b values from the converged FEA solutions, labeled as $C_{b\ exact}$, to the C_b obtained from the design expressions (i.e., $C_{b\ exact}/C_b$) for all of the cross sections and W values considered in this study. Emphasis is given to having an unbiased, evenly distributed sampling throughout the design space of which Figures 7 through 12 are a subset. The main box of the boxplots conveys the 25th percentile, median, and 75th percentile values for $C_{b\ exact}/C_b$, and the upper and lower whiskers convey the maximum and minimum $C_{b\ exact}/C_b$ in each of the data sets. As discussed in the previous section, W is varied in this work by considering L_b/h_o values of 5, 10, 20, and 30, and by analyzing members with L_b/h_o = 10 taking J = 0. Figure 13 corresponds to the linear moment cases (ξ = 0.0), while Figure 14 corresponds to all the nonlinear moment cases, both concentrated transverse load at the middle of the unbraced length and uniformly distributed transverse load throughout the unbraced length.

The plots in Figures 13 and 14 are arranged in five columns corresponding to ρ = 0.1, 0.3, 0.5, 0.7, and 0.9, and the rows correspond to L_b/h_o ranging from the maximum of 30 at the bottom of the array down to L_b/h_o = 5 in the next to top row of the array. As discussed previously, L_b/h_o = 30 gives the smallest values of W (Equation 25) for the selected member cross sections, and L_b/h_o = 5 gives the largest finite values of W. The range of W values corresponding to each row of the plot arrays is summarized on the right-hand side of the figure. The specific W values for the different cases also are summarized in Table 1. The top row of the array of plots in Figures 13 and 14 corresponds to the idealized case in which the St. Venant torsion constant, J, is taken equal to zero. This gives an effective W value of infinity.

Tables 2 and 3 summarize the statistics for $C_{b\ exact}/C_b$ corresponding to all of the data from the box plot arrays of

Figures 13 and 14. The dispersion in the ASC and AASHTO data is substantial. The ASC $C_{b\ exact}/C_b$ data is essentially tri-modal. That is, the $C_{b\ exact}/C_{b\ ASC}$ values coalesce largely into three groups: results for $R_m > 1.0$, results for $R_m < 1.0$, and results for $R_m = 1.0$. Furthermore, the $C_{b\ exact}/C_{b\ AASHTO}$ data is essentially bimodal, coalescing largely into two groups: results where $C_{b\ AASHTO}$ is simply taken equal to 1.0 and results where $C_{b\ AASHTO}$ is greater than 1.0. From an overall perspective, the recommended method clearly outperforms both of the current methods. However, even for the recommended method, there are some cases where the converged numerical benchmark $C_{b\ exact}$ values are overpredicted. These are discussed further in the following sections. First, it is important to explain the overall behavior of each of the expressions for C_b.

One additional column is added to Tables 2 and 3 to address the question of how the quarter-point equation given by the AISC *Specification* Equation F1-1 performs if applied in the same way that the Wong and Driver formula, ASC Equation C-F1-2b, is adapted in Equation 10. This column is labeled "Recommended (ASC)." One can observe that the Wong and Driver equation offers some minor improvement in the overall statistics relative to the AISC *Specification* Equation F1-1.

Behavior of the ASC C_b Equations

The ASC design expressions (ASC Equation C-F1-3 and Equation 1) exhibit the following behavior with variations

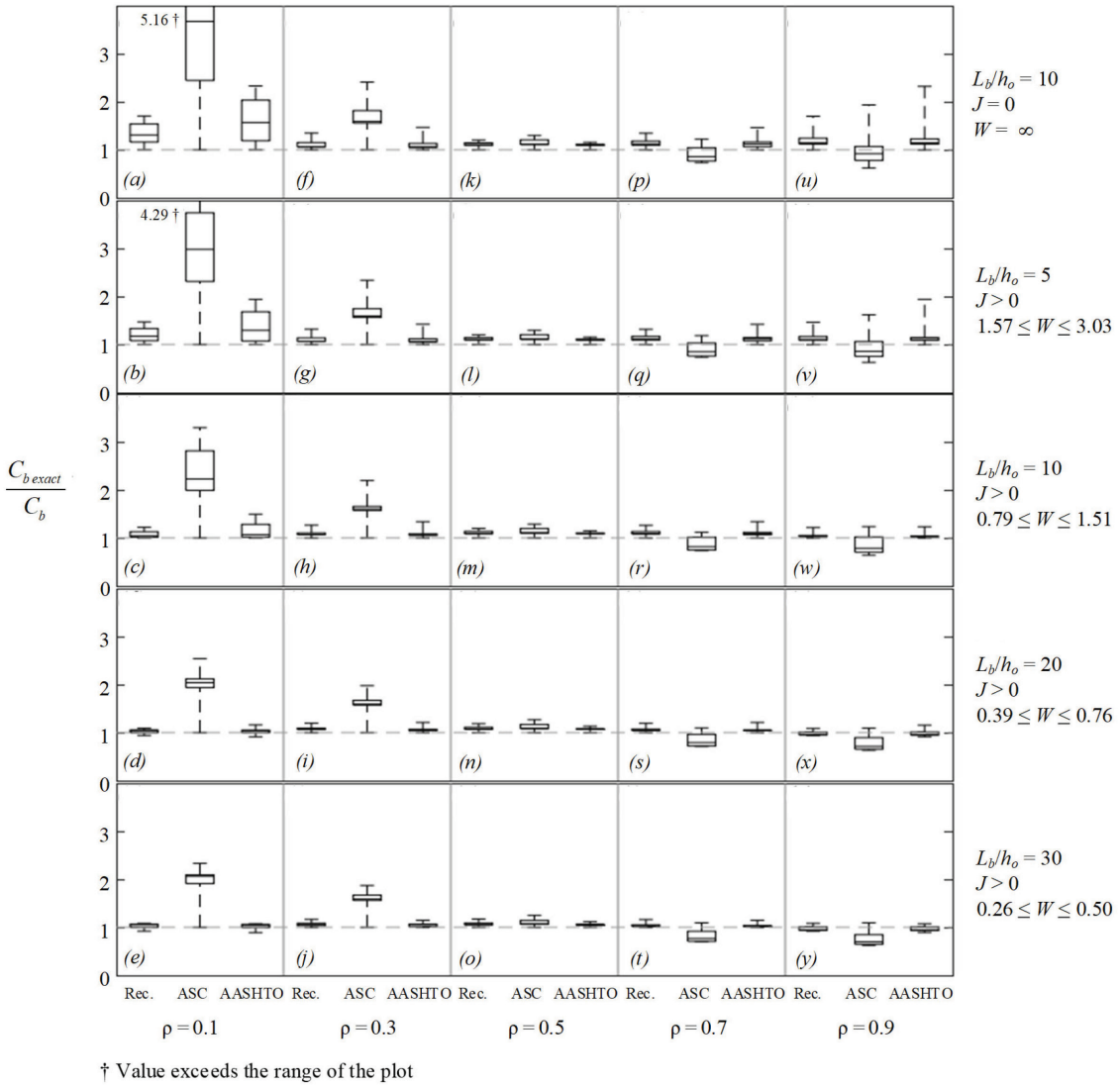

Fig. 13. Boxplots of $C_{b\ exact}/C_b$ *for linear moment cases.*

in the independent variable ρ for the members considered in this study:

- For all single-curvature bending cases, R_m = 1.0 from Equation 1a.
- For the reverse-curvature bending cases with ρ = 0.1, $I_{y.top} = 0.1\, I_y$:
  - When ξ > 0.0, the transverse loading is "downward"; therefore, $I_{y.opp} = I_{y.top} = 0.1\, I_y$ and R_m = 0.520 from Equation 1b.
  - When ξ < 0.0, the transverse loading is "upward"; therefore, $I_{y.opp} = I_{y.bot} = 0.9 I_y$ and R_m = 2.118 from Equation 1b.
- For the reverse-curvature bending cases with ρ = 0.3, $I_{y.top} = 0.3\, I_y$:
  - When ξ > 0.0, the transverse loading is "downward"; therefore, $I_{y.opp} = I_{y.top} = 0.3 I_y$ and R_m = 0.680 from Equation 1b.
  - When ξ < 0.0, the transverse loading is "upward"; therefore, $I_{y.opp} = I_{y.bot} = 0.7 I_y$ and R_m = 1.479 from Equation 1b.

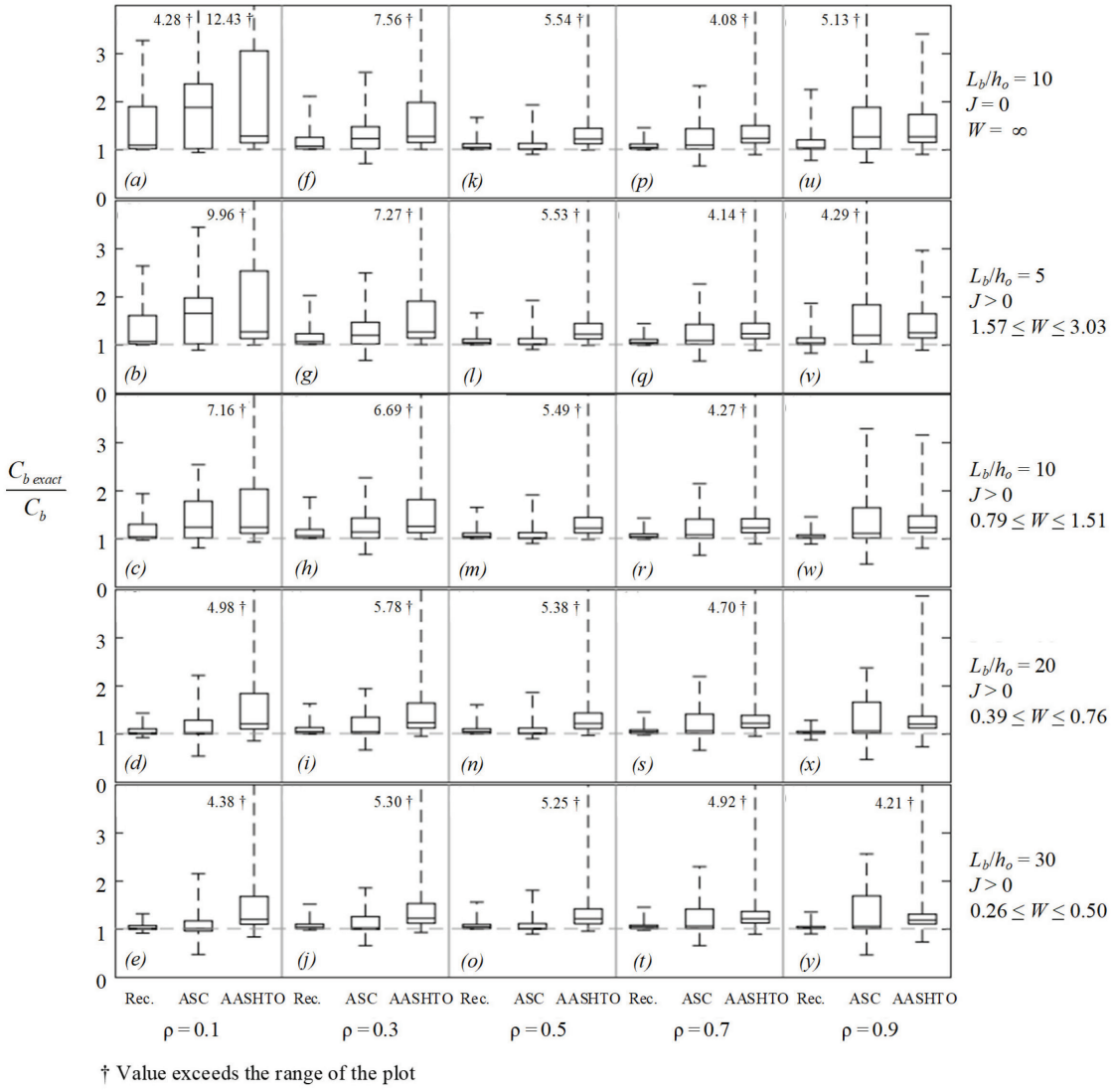

Fig. 14. Boxplots of $C_{b\,exact}/C_b$ *for nonlinear moment cases—concentrated transverse load at the middle of the unbraced length and uniformly distributed transverse load.*

Table 4. Values of R_m as a Function of ρ and ξ			
$\rho = I_{y.top}/I_y$	ξ	$I_{y.opp}/I_y$	R_m
0.1	≥0.0	0.1	0.520
0.1	<0.0	0.9	2.118
0.3	≥0.0	0.3	0.680
0.3	<0.0	0.7	1.479
0.5	All values	0.5	1.000
0.7	≥0.0	0.7	1.479
0.7	<0.0	0.3	0.680
0.9	≥0.0	0.9	2.118
0.9	<0.0	0.1	0.520

- For the reverse-curvature bending cases with ρ = 0.7, $I_{y.top} = 0.7I_y$:
  - When ξ > 0.0, the transverse loading is "downward"; therefore, $I_{y.opp} = I_{y.top} = 0.7I_y$ and $R_m = 1.479$ from Equation 1b.
  - When ξ < 0.0, the transverse loading is "upward"; therefore, $I_{y.opp} = I_{y.bot} = 0.3I_y$ and $R_m = 0.680$ from Equation 1b.
- For the reverse-curvature bending cases with ρ = 0.9, $I_{y.top} = 0.9I_y$:
  - When ξ > 0.0, the transverse loading is "downward"; therefore, $I_{y.opp} = I_{y.top} = 0.9I_y$ and $R_m = 2.118$ from Equation 1b.
  - When ξ < 0.0, the transverse loading is "upward"; therefore, $I_{y.opp} = I_{y.top} = 0.1I_y$ and $R_m = 0.520$ from Equation 1b.

In the limit ξ = 0.0, there is no transverse load, and therefore, one can infer that there is no gravity load direction and that R_m should be taken equal to 1.0. However, it is common that the self-weight moments in horizontal members may be small compared to the moments from the applied loads. In these cases, there is indeed a gravity load direction, but the moment diagrams are linear for all practical purposes. The results plotted in Figure 7 are based on this situation. The gravity direction is taken as downward, and the "top" flange is taken as the "opposite" flange in this case.

The variations of R_m with ρ and ξ are summarized in Table 4. These results are important toward understanding the various discontinuities in the ASC C_b curves shown in Figures 7 through 12.

Generally, discontinuities in the ASC C_b values can occur where:

1. The moment diagram changes from single-curvature to reverse-curvature bending. The values of α and ξ corresponding to this occurrence are highlighted, and the horizontal position on the plots where this occurs are clearly marked in Figures 8 through 12. The following are examples of these situations:
   - Considering Figure 7(a), where ξ = 0 but it is assumed that there is a small downward transverse load on the members, the unbraced length goes into reverse-curvature bending when $\alpha = M_L/M_R$ becomes negative. As such, R_m changes from 1.0 for positive α to 0.520 for negative α. This causes an abrupt downward shift of the ASC C_b curve for negative α.
   - A similar discontinuity occurs in Figure 7(d), where R_m changes from 1.0 for positive α to 1.479 for negative α, causing an abrupt upward shift in the ASC C_b curve for negative α.
   - Considering Figure 11(a), R_m changes from 1.0 for ξ ≥ –1.0 to 0.680 for ξ < –1.0, causing an abrupt downward shift in the ASC C_b values for ξ < –1.0.

   A number of other similar discontinuities appear throughout Figures 8 through 12.
2. The unbraced length is subjected to reverse-curvature bending, due to the values of the end moments (i.e., α = 0.5 or –1.0), and the direction of the transverse loading changes from positive ξ (downward), to negative ξ (upward). The following are examples of these situations:
   - Considering Figure 8(d), R_m changes from 0.520 for ξ > 0.0 to 2.118 for ξ < 0.0. The magnitude of the shift in the ASC C_b curve in this case is limited by the cap of 3.0 in the ASC Equation CF1-3.
   - Considering Figure 11(d), R_m changes from 1.479 for ξ > 0.0 to 0.680 for ξ < 0.0. The ASC C_b curve shifts in the opposite direction with increasing ξ in this case because the top flange is larger than the bottom flange, rather than smaller, while the variation in the

loading direction from downward to upward is the same. Again, the magnitude of the shift in the ASC C_b curve is limited by the maximum cap of 3.0 in the ASC Equation C-F1-3.

Again, a number of other similar discontinuities appear throughout Figures 8 to 12.

Slein et al. (2021) also discuss the attributes of the calculations producing discrete changes in the slope of the ASC and other C_b curves in Figures 7-12, plotted versus $\alpha = M_L/M_R$.

Clearly the discontinuities in the ASC C_b values as a function of α and ξ are nonphysical. For ρ values significantly different than 0.5, these discontinuities can introduce both substantial conservatism and unconservatism into the ASC LTB predictions. The largest conservatism in the ASC calculations tends to occur for cases where there is only a minor amount of reverse-curvature bending causing compression on the smaller flange. However, the R_m calculation (Equations 1) gives a substantial indiscriminant reduction in the C_b value without considering the actual pattern of tension and compression within the smaller flange. The largest unconservatism in the ASC calculations tends to occur for cases where there is only a minor amount of reverse-curvature bending causing compression on the larger flange. However, the R_m calculation (Equations 1) gives a substantial indiscriminant increase in the C_b value without considering the actual pattern of tension and compression within the larger flange. Nevertheless, one can observe that the discontinuities in the ASC C_b values do follow the trends in the benchmark $C_{b\ exact}$ curves to some extent for cases subjected to significant transverse loads and significant simply supported moments, M_{ss} (Equations 17 and 18). This is evidenced by the larger ASC C_b predictions, due to larger R_m for negative ξ values, in Figures 8 and 9, and the smaller ASC C_b predictions, due to smaller R_m for negative ξ values, in Figures 11 and 12.

It should be noted that as a check of the benchmark thin-walled open-section beam theory solutions from SABRE2 (White et al., 2021) employed in this paper, as well as to check the intended application of the ASC C_b expressions, the authors analyzed all the cases corresponding to loadings applied at the web mid-height from Helwig et al. (1997). A close match was obtained with the original solutions by Helwig et al. The difference in the accuracy of the results for the broader studies conducted in this work versus the original studies by Helwig et al. appears to be due to the fact that only simply supported, fixed-fixed and propped cantilever beams were considered in the development of the ASC R_m factor by Helwig et al. As stated previously, the solutions in this paper focus on loadings involving a more general variation of the end moments. The reader is referred to Wong and Driver (2010) for additional solutions involving simply supported beams.

For the concentrated transverse load cases, shown in Slein et al. (2021), the fixed-fixed and propped cantilever end conditions correspond to $\xi = -2$ and -1.33 for $\alpha = -1.0$ and 0.0, respectively. For the uniformly distributed load cases shown in Figures 8 through 12, the fixed-fixed and propped cantilever end conditions correspond to $\xi = -1.5$ and -1.0 in plots (a) and (c), respectively. One can observe that the predictions by the ASC equations are relatively accurate for these specific load cases.

Behavior of the AASHTO C_b Equations

Different values are calculated for $C_{b.top}$ and $C_{b.bot}$ in the AASHTO procedure (see Equation 7). This practice is aimed at accounting for the different patterns of compression and tension in the separate flanges for cases involving moment reversal. However, due to the different $C_{b.top}$ and $C_{b.bot}$ values calculated using this approach, this method produces a discontinuity in the governing C_b value when there is a change in the flange governing the calculation of γ_{eLTB}. This behavior does not occur with the other methods evaluated in this study. For the other methods (i.e., the ASC method, the recommended method, and the benchmark calculations from elastic linear buckling analysis), the C_b curves are continuous at any α or ξ values where there is a change in the governing flange.

This behavior of the AASHTO equations appears at $\alpha = -3.45$ in Figure 7(a), at $\xi = -0.74$ in Figure 9(e), at $\xi = -0.66$ in Figure 10(d), and at $\xi = +0.74$ in Figure 11(e).

The AASHTO procedure also gives a sharp discontinuity in its C_b value at any ξ where the maximum moment within the unbraced length becomes larger than the maximum end moment of the same sign. At these values of ξ, the AASHTO method switches from a calculation of $C_b > 1$ based on Equation 9 to the simplistic estimate of $C_b = 1$. This occurs at $\xi = -1.66$ in Figure 8(e), at $\xi = -1.58$ in Figure 9(c), at $\xi = -1.06$ in Figure 9(d), at $\xi = -1.52$ in Figure 10(b), at $\xi = -1.07$ in Figure 10(c), at $\xi = -1.16$ in Figure 11(b), and at $\xi = -0.80$ in Figure 11(c).

These discontinuities occur across a broad range of ρ, α, and ξ values, and it can be observed that, generally, they are appropriate and a part of the ability of the AASHTO method to account for the different patterns of compression and tension in the separate flanges in unbraced lengths subjected to reverse-curvature bending. That is, the AASHTO C_b curves tend to follow the trends in the increasing or decreasing values of the benchmark solutions. However, the physical behavior captured by the benchmark solutions does not involve any discontinuities in the C_b values. As such, any solution having sharp discontinuities will exhibit inaccuracies at these locations. In the case of the AASHTO

method, these inaccuracies are always conservative for the plots shown in this work. Nevertheless, the simplistic AASHTO solution of taking $C_b = 1.0$ when the maximum moment within the unbraced length is larger than the maximum end moment of the same sign is a critical flaw that is acknowledged in the AASHTO Commentary. This flaw makes the AASHTO method overly conservative for spans that have a limited number of intermediate brace points. These situations may exist in short-span bridges and in longer-span bridges during construction.

Behavior of the Recommended C_b Calculations

Considering Figures 7 through 12, one can observe that the recommended C_b calculation procedure does not exhibit any discontinuities in its value as a function of ρ, α, or ξ. The recommended C_b predictions generally follow the trends in the benchmark solutions quite well. The result from the recommended C_b calculations tends to be conservative in the vicinity of the largest benchmark and estimated C_b values. This is an attribute of the calibration of the ASC Equation C-F1-2b by Wong and Driver. As presented in detail in the subsequent discussions, members with large contributions from St. Venant torsion relative to the warping torsion tend to have smaller $C_{b\ exact}$ values. These cases are encountered at larger L_b/h_o for a given member cross section and for heavy column type members, which generally have large St. Venant torsional rigidity, GJ, compared to their warping rigidity, EC_w. In essence, these are cases with the smallest W values (see Equation 25). Since the design expressions only account for variations in the moment along the unbraced length, and do not account for this significant attribute of the elastic LTB behavior, they need to be calibrated to give accurate results for practical situations having the smallest W.

At the opposite extreme, singly symmetric members with (1) the St. Venant torsion constant idealized as zero (such that there is no assistance from St. Venant torsion in resisting elastic LTB), (2) $\rho = 0.1$ (i.e., a small "top" flange), and (3) a moment diagram producing compression within the larger flange within the span but where the smaller flange loaded in maximum compression at one or both braced points governs [corresponding to the moment diagrams for $\xi = -1.5$ in Figure 5(f), or for $\xi = -1.2$ in Figure 5(g)], the $C_{b\ exact}$ values are a whopping 12.43 and 12.83, respectively! For these cases, the recommended calculations give $C_b = 3.94$ and 3.95, respectively. The latter of these cases corresponds to the largest $C_{b\ exact}/C_{b\ Rec}$ of 3.26 for the recommended calculations shown in Figure 14(a) and listed in Table 3. The ASC equations take on their maximum value of 3.0 for this case, resulting in $C_{b\ exact}/C_{b\ ASC} = 12.83/3.0 = 4.28$, whereas the AASHTO procedure gives only $C_b = 1.3$ for this case, resulting in $C_{b\ exact}/C_{b\ AASHTO} = 12.83/1.3 = 9.87$ (the first of these cases gives the largest conservatism of the AASHTO calculations of $C_{b\ exact}/C_{b\ AASHTO} = 12.43/1.0 = 12.43$).

Therefore, the recommended procedure tends to be conservative at large C_b values for members with unbraced lengths having large values of W. Nevertheless, an estimated C_b of 3.95 will often place the LTB resistance, M_n, at the "plateau" strength. Hence there is limited need for more liberal estimates of these very large C_b values. The reader can observe from Figure 8 that for the singly symmetric cross sections targeted in this study, $L_b/h_o = 10$, and with similar moment diagrams compared to those just discussed, the largest benchmark $C_{b\ exact}$ values are between 5.0 and 7.3, and these trends are captured conservatively by the recommended C_b calculations.

There is a specific unusual case for $J = 0$ ($W = \infty$) and $\rho = 0.9$ where there is an extreme sensitivity in the calculation of the governing elastic LTB resistance and the recommended equations exhibit a minimum $C_{b\ exact}/C_{b\ Rec}$ of 0.769 [see Figure 14(u) and Table 3]. This case is discussed in detail in the following section.

Consideration of Cases with the Smallest $C_{b\ exact}/C_b$ for the Different C_b Design Expressions

By far, the most important attribute of all structural design procedures is that they do not result in situations in which structural capacities are significantly overestimated. Therefore, it is most important that the subject design calculations be scrutinized for any situations where $C_{b\ exact}/C_b$ is significantly less than 1.0.

Figure 15(a) provides a plot from the complete set of studies conducted in this research that exhibits the smallest values of $C_{b\ exact}/C_b$ specifically for linear moment diagrams for all the considered design estimates. Figures 15(b) through 15(d) show the specific worst-case loadings, their moment diagrams, other pertinent parameters, and the corresponding C_b design estimates. For these cases, $L_b/h_o = 30$ and $\rho = 0.9$, resulting in the minimum values for W (see Table 1). A small downward distributed load, corresponding to $\xi = 0.01$, is considered. This makes the moment diagrams slightly nonlinear. In the cases labeled in Figure 15(a), the ASC procedure significantly overestimates the benchmark solution by applying $R_m = 2.118$ for $\alpha < 0$. This gives a predicted ASC C_b equal to the ASC maximum limit of 3.0. The specific cases labeled in Figure 15(a) are as follows:

- The smallest $C_{b\ exact}/C_{b\ ASC} = 0.608$ occurs for negative α values close to zero (i.e., where there is only a minor amount of reverse-curvature bending causing compression in the larger top flange). This is labeled as Case 1 in Figure 15(a). The specific parameters and C_b values for this case are shown in Figure 15(b).
- $C_{b\ exact}/C_{b\ ASC}$ also becomes quite small at larger negative α values, leading to $C_{b\ exact}/C_{b\ ASC} = 0.624$ at $\alpha = -5$). This is labeled as Case 2 in Figure 15(a) and the specific

parameters and C_b values are summarized for this case in Figure 15(c).

- The recommended and the AASHTO C_b calculations both follow the benchmark $C_{b\ exact}$ trends in Figure 15(a). However, they both tend to slightly overshoot the $C_{b\ exact}$ values for cases with $\alpha < -1.0$. The smallest $C_{b\ exact}/C_{b\ AASHTO}$ of 0.892 occurs at $\alpha = -1.7$, where $C_{b\ AASHTO}$ starts to reduce below its maximum limit of 2.5. This is labeled as Case 3 in Figure 15(a), and the specific parameters and C_b values are summarized for this case in Figure 15(d). It should be noted that lowering the cap on $C_{b\ AASHTO}$ from 2.5 to 2.3 would only shift the point at which $C_{b\ AASHTO}$ starts to reduce below the maximum limit to $\alpha = -2.2$ in Figure 15(a), and would result in an improvement in the smallest $C_{b\ exact}/C_{b\ AASHTO}$ to only 0.914.
- The recommended method has the smallest unconservative error of all the considered design procedures in Figure 15(a), correctly following the trends in the benchmark $C_{b\ exact}$ curve but giving a smallest $C_{b\ exact}/C_{b\ Rec}$ of 0.920 at $\alpha = -1.5$. This specific case is not illustrated in Figure 15, but it is very similar to the case in Figure 15(d). This amount of unconservatism for the most extreme case of large ρ and small W values is considered acceptable.

Figure 15 can be compared to Figure 7(e) to gain a perspective of the influence of the extreme value of $L_b/h_o = 30$ compared to the intermediate value of $L_b/h_o = 10$ for this problem. One can observe that in Figure 7(e), the recommended C_b calculation is always slightly conservative compared to the benchmark $C_{b\ exact}$ values.

Figure 16 provides a plot from the complete set of studies conducted in this research and documented in Slein et al. (2021). This figure shows Case 4, a concentrated transverse load case exhibiting the smallest values of $C_{b\ exact}/C_b$ from the ASC calculations for the nonlinear moment diagrams considered. The specific parameters and C_b values for Case 4 are detailed in Figure 16(b). In Figure 16, again $L_b/h_o = 30$ and $\rho = 0.9$, resulting in the minimum values for W. The following observations can be gleaned from this figure:

- The ASC method properly scales down its C_b values by $R_m = 0.520$ for negative ξ values. This results in substantial conservatism between $\xi = 0.0$ and -0.5 and produces C_b values less than 1.0 for $\xi < -0.7$.
- However, for $\xi > 0$, the ASC method improperly scales up its C_b values by $R_m = 2.118$, with a maximum cap on its C_b of 3.0. This results in the minimum $C_{b\ exact}/C_{b\ ASC}$ of 0.454 at $\xi = 0.7$, which is labeled as Case 4. This case is particularly worrisome since $C_{b\ exact}$ is only 1.22, while $C_{b\ ASC}$ is 2.67.
- It can be observed that the recommended and the AASHTO C_b calculations both provide a reasonably accurate estimate of the benchmark $C_{b\ exact}$ values throughout the range $-2.0 \le \xi \le 2.0$ for this problem, with the recommended procedure giving a highly accurate prediction of the shape of and the values from the $C_{b\ exact}$ curve.

Figure 16(a) may be compared to the corresponding predictions for $L_b/h_o = 10$ [see Slein et al. (2021)] to gain a perspective of the influence of $L_b/h_o = 30$ compared to more intermediate length-to-depth ratios for this problem. For $L_b/h_o = 10$, the recommended C_b calculation is accurate to slightly conservative compared to the benchmark $C_{b\ exact}$ values for all of the studied ξ values.

Figure 17 shows another example from the studies conducted in this research that exhibits small values of $C_{b\ exact}/C_b$ from the ASC procedure for nonlinear moment diagrams. This plot corresponds to $L_b/h_o = 30$, $\rho = 0.3$, and $\alpha = -1.0$. Considering Figure 17(a), the ASC procedure appropriately scales down its C_b value by $R_m = 0.680$ for $\xi > 0$, although this leads to significantly conservative estimates for small ξ values. However, its use of $R_m = 1.479$ for negative ξ results in a low $C_{b\ exact}/C_{b\ ASC}$ of 0.650 at $\xi = -1.4$. This specific loading and geometry is labeled as Case 5 and is detailed in Figure 17(b). Again, the fact that $C_{b\ exact}$ is only 1.27 but $C_{b\ ASC}$ is significantly larger at 1.95 is troubling. It should be noted that this problem is equivalent to $L_b/h_o = 30$, $\rho = 0.7$, equal but opposite end moments corresponding to $\alpha = -1.0$, and a downward load corresponding to $\xi = +1.4$.

Figure 17(a) may be compared to the corresponding predictions for $L_b/h_o = 10$ [see Slein et al. (2021)] to gain a perspective of the influence of the extreme $L_b/h_o = 30$ compared to more intermediate length-to-depth ratios for this problem. Again, for $L_b/h_o = 10$, the recommended C_b calculation is accurate to slightly conservative compared to the benchmark $C_{b\ exact}$ values for all of the studied ξ values. The $C_{b\ exact}$ for $L_b/h_o = 10$ increases significantly for increasing ξ values starting from the local minimum $C_{b\ exact}$ at $\xi = -2.0$.

Figure 18 highlights another case (Case 6) similar to that of Case 5 in Figure 17, but where the $C_{b\ exact}/C_{b\ ASC}$ is particularly small at $\xi = -2.0$. This is due to a smaller ρ of 0.1 in this problem. The $C_{b\ ASC}$ for Case 6 is 2.79, whereas $C_{b\ exact}$ is only 1.30. In addition, one can observe that the AASHTO predictions are quite conservative for $\xi < -0.7$ in Figure 18(a). Furthermore, the recommended calculations range from highly accurate, to slightly conservative, to slightly overestimating the benchmark solutions in this plot.

Figure 18 can be compared to the corresponding predictions for $L_b/h_o = 10$ [see Slein et al. (2021)] to gain a perspective of the influence of the extreme $L_b/h_o = 30$ compared to intermediate length-to-depth values for this problem. For

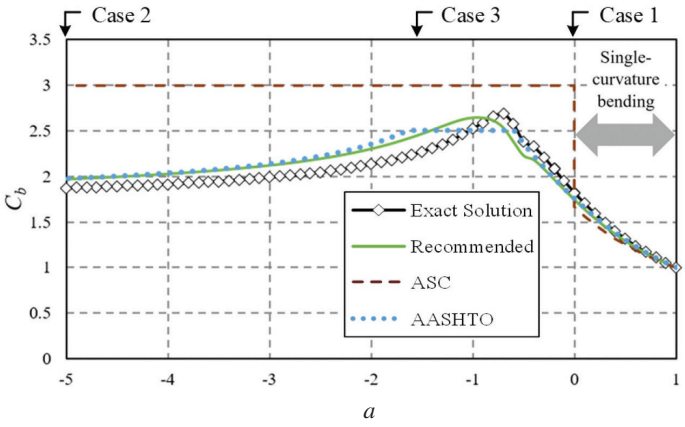

(a) C_b *versus* α

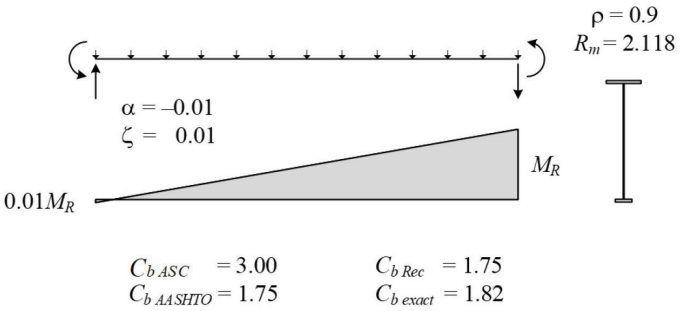

(b) *Case 1 parameters and* C_b *values*

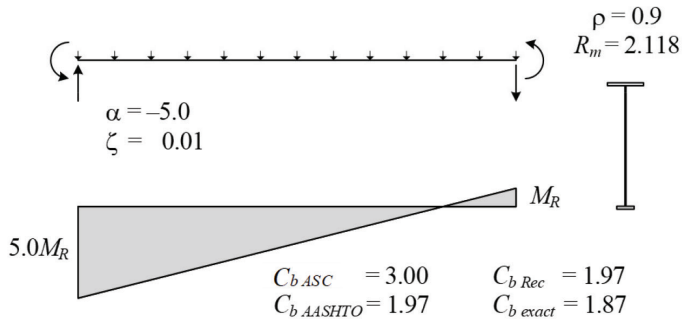

(c) *Case 2 parameters and* C_b *values*

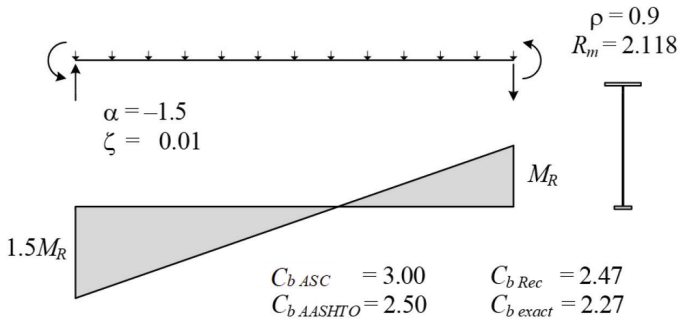

(d) *Case 3 parameters and* C_b *values*

Fig. 15. Cases exhibiting smallest $C_{b\,exact}/C_b$ *for the ASC, AASHTO, and recommended procedures for linear moment:* $L_b/h_o = 30$, $\rho = 0.9$ ($C_{b\,exact}/C_{b\,ASC} = 0.608$ *at* $\alpha = 0$, $C_{b\,exact}/C_{b\,AASHTO} = 0.892$ *at* $\alpha = -1.7$, $C_{b\,exact}/C_{b\,Rec} = 0.920$ *at* $\alpha = -1.5$).

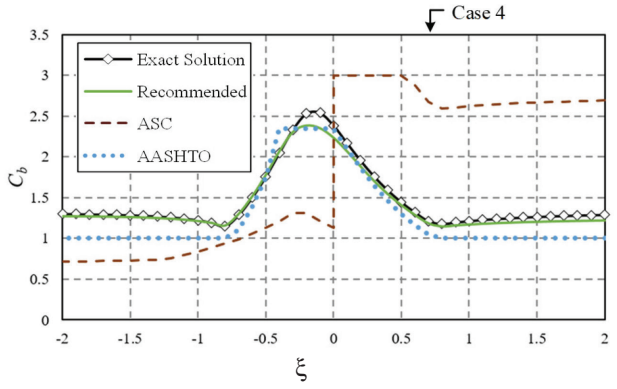

(a) C_b *versus* ξ

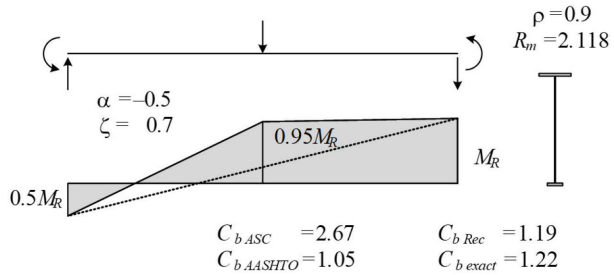

(b) *Case 4 parameters and* C_b *values*

Fig. 16. Worst-case $C_{b\,exact}/C_b$ *for ASC procedure, nonlinear moment—Case 4: concentrated transverse load,* $L_b/h_o = 30$, $\rho = 0.9$, $a = -0.5$ ($C_{b\,exact}/C_{b\,ASC} = 0.454$ *at* $\xi = 0.7$).

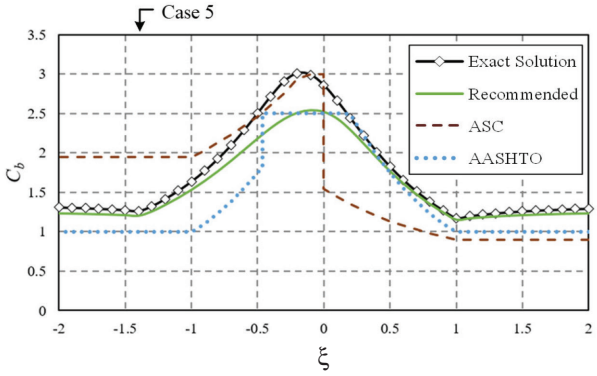

(a) C_b *versus* ξ

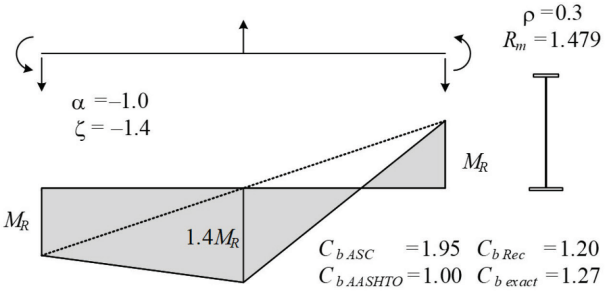

(b) *Case 5 parameters and* C_b *values*

Fig. 17. Illustration of small $C_{b\,exact}/C_b$ *for ASC procedure, nonlinear moment—Case 5: concentrated transverse load,* $L_b/h_o = 30$, $\rho = 0.3$, $\alpha = -1.0$ ($C_{b\,exact}/C_{b\,ASC} = 0.650$ at $\xi = -1.4$).

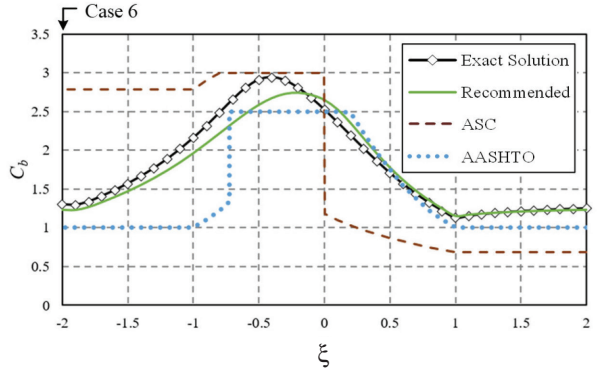

(a) C_b *versus* ξ

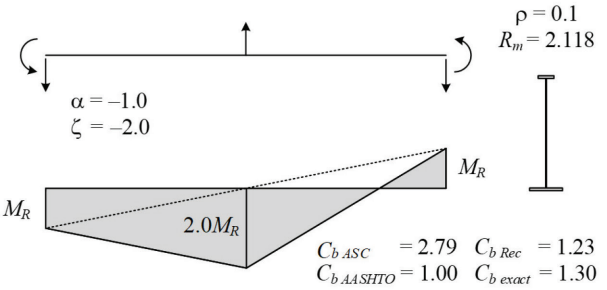

(b) *Case 6 parameters and* C_b *values*

Fig. 18. Example small $C_{b\,exact}/C_b$ *for ASC procedure, nonlinear moment—Case 6: concentrated transverse load,* $L_b/h_o = 30$, $\rho = 0.1$, $\alpha = -1.0$ ($C_{b\,exact}/C_{b\,ASC} = 0.466$ at $\xi = -2.0$).

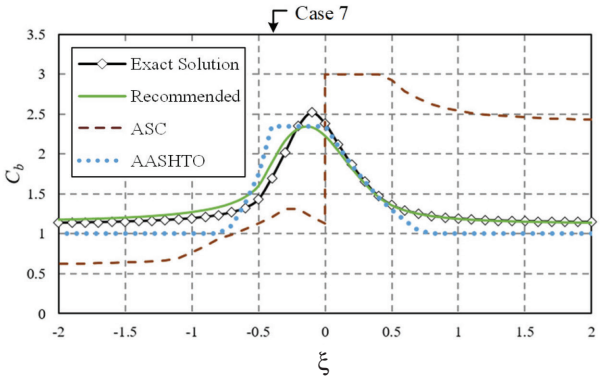

(a) C_b *versus* ξ

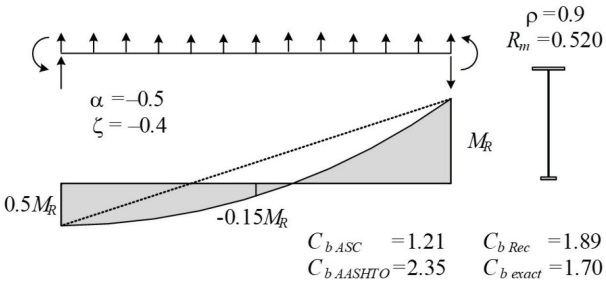

(b) *Case 7 parameters and* C_b *values*

Fig. 19. Worst-case $C_{b\,exact}/C_b$ *for AASHTO procedure, nonlinear moment—Case 7:* $L_b/h_o = 30$, $\rho = 0.9$, $\alpha = -0.5$, *distributed transverse load* ($C_{b\,exact}/C_{b\,AASHTO} = 0.722$ at $\xi = -0.4$).

$L_b/h_o = 10$, the recommended method gives accurate to conservative predictions for all the cases.

Figure 19 highlights Case 7, which has the smallest values of $C_{b\ exact}/C_b$ from the AASHTO procedure for the nonlinear moment diagrams considered. Figure 19(a) corresponds to $L_b/h_o = 30$, $\rho = 0.9$, $\alpha = -0.5$, and uniformly distributed transverse load. The AASHTO calculations provide a reasonable capture of the benchmark solutions in Figure 19(a). However, at the Case 7 value of $\xi = -0.4$, where $C_{b\ AASHTO}$ starts to reduce below the value of 2.35, due to a change in location of the moment causing the maximum compression on the smaller bottom flange from the left-hand end to the interior of the span, $C_{b\ exact}/C_{b\ AASHTO} = 0.722$. Changing the maximum cap on the AASHTO results to $C_b = 2.3$ does little to change this overestimation of the benchmark solution.

It should be noted that Case 7 is equivalent to $L_b/h_o = 30$, $\rho = 0.1$, $\alpha = -2.0$, and a downward load corresponding to $\xi = +0.8$. In fact, for any of the cases presented in Figures 7 through 21, an equivalent case is produced by:

- Negating the moment diagram.
- Setting ρ to $(1 - \rho)$.
- Setting ξ to $-\xi/\alpha$.
- Setting α to $1/\alpha$.

The parameters $\rho = 0.1$, $\alpha = -2.0$, and $\xi = +0.8$ are representative of a potential unbraced length adjacent to an interior support in a continuous-span girder with a smaller top flange, large negative moment at the interior support on the left-hand end, downward distributed load, and a smaller positive moment equal to one-half of the maximum negative end moment at the right-hand end of the unbraced length. Appendix B illustrates calculations for a similar bridge girder having $L_b/h_o = 15$, $\rho = 0.229$, $\alpha = -2.0$, and $\xi = +0.5$.

Figure 19 can be compared to Figure 12(d) to gain a perspective of the influence of the extreme $L_b/h_o = 30$ compared to the more intermediate value of $L_b/h_o = 10$ for this problem. One can observe that in Figure 12(d), the maximum ove-estimation of the benchmark solution by the AASHTO result (at $\xi = -0.3$) is slightly smaller than in Case 7.

Figure 20 highlights Case 8, which exhibits the smallest values of $C_{b\ exact}/C_b$ from the recommended method for the nonlinear moment diagrams considered. This figure corresponds to a very different set of loadings and geometry compared to those discussed in the preceding text. Figure 20 corresponds to $L_b/h_o = 10$, but with J taken equal to zero, which makes the benchmark solution essentially independent of L_b/h_o. In Case 8, where $\alpha = 0.0$ (zero moment at the left-hand end), the unbraced length is subjected to a concentrated transverse load at its mid-length such that, given $\xi = -0.5$, the entire left half of the unbraced length is subjected to zero moment while the right half is subjected to a linearly varying moment from zero at the mid-span to a maximum value at the right-hand support. For this case, the unbraced length is in single-curvature bending with the flexural compression occurring in the larger top flange. As such, $C_{b\ Rec}$ is relatively large at 2.83. The ASC calculations give a $C_{b\ ASC}$ of 3.0. However, for decreasing ξ values infinitesimally smaller than −0.5, the unbraced length is subjected to reverse-curvature bending with larger and larger compression in the member's small bottom flange on its left half. This results in a dramatic reduction in the C_b values for decreasing ξ slightly less than −0.5. Both the recommended and ASC C_b methods capture this substantial sensitivity in the LTB resistance.

In the benchmark solution for this problem, the elastic LTB resistance starts to reduce significantly with decreasing ξ values for $\xi < -0.4$. It appears that the behavior is such that the tension added to the small bottom flange at $\xi = -0.4$ helps stiffen that flange against lateral displacement,

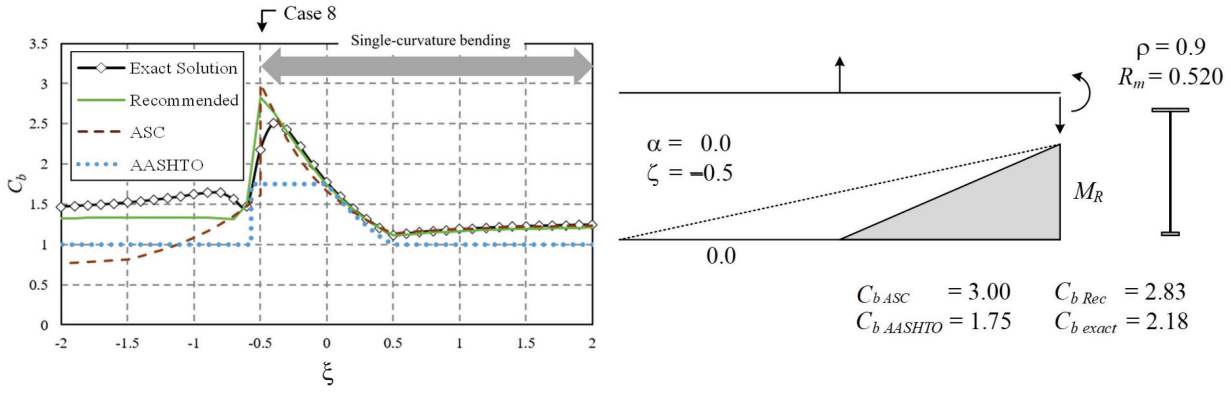

(a) C_b *versus* ξ *(b) Case 8 parameters and* C_b *values*

Fig. 20. Worst-case $C_{b\ exact}/C_b$ *for recommended procedure, nonlinear moment—Case 8:* $L_b/h_o = 10$, $J = 0$, $\rho = 0.9$, $\alpha = 0.0$, *concentrated transverse load at the middle of the unbraced length* ($C_{b\ exact}/C_{b\ Rec} = 0.769$ *at* $\xi = -0.5$).

resulting in a larger LTB resistance, although the larger top flange is seeing larger flexural compression for this case. The buckling mode for $\xi = -0.5$ shows substantially larger lateral movement of the bottom flange within the left-half of the beam compared to the result for $\xi = -0.4$ (see Figure 21).

The sensitivity at $\xi = -0.5$ for this problem results in a $C_{b\,exact}/C_{b\,Rec} = 0.769$. It should be noted that $C_{b\,exact}/C_{b\,ASC} = 0.725$ at this value of ξ.

Figure 20(a) may be compared to the corresponding concentrated transverse load plot with J included [see Slein et al. (2021)] to gain a perspective of the influence the extreme assumption of $J = 0$. With J included, the recommended procedure gives a reasonably accurate characterization of $C_{b\,exact}$ for the entire range of the ξ values. The idealized elastic LTB solution assuming $J = 0$ is a common one employed in the ASC and AASHTO *Specifications* for slender-web members. This idealization is employed to provide some accounting for the potential reductions in the LTB resistance of these types of members due to web distortion. However, there is always some influence from St. Venant torsion, which tends to make the elastic LTB predictions assuming $J = 0$ slightly conservative. As can be seen from the minimum whisker for the recommended method in Figures 14(u) and 14(v), the consideration of a relatively large but finite W value measurably reduces the unconservative errors shown in Figure 20. The minimum $C_{b\,exact}/C_{b\,Rec}$ in Figure 14(v) is 0.836. In addition, for $L_b/h_o = 5$, the LTB resistance will tend to be in the inelastic buckling range, which tends to further reduce the effect of potential overestimation of the benchmark elastic LTB resistance for the locally sensitive Case 8 in Figure 20.

Consideration of C_b Design Estimates for Long Heavy Column Members

The authors submit that the targeted doubly symmetric girder cross sections based on Figure 6, and the singly symmetric girder cross sections obtained after reducing the flange widths from the base values specified in this figure, combined with a maximum $L_b/h_o = 30$, provide reasonable minimum W values (see Table 1) representative of practical steel beam and girder designs. However, for heavy column sections, smaller W values are possible. Based on the synthesis in Figures 13 and 14, it is clear that the smallest benchmark $C_{b\,exact}$ values are obtained in cases where W is the smallest. As such, Slein et al. (2021) show additional studies investigating the behavior for W14×873 members with $L_b/d = 30$ as a representative extreme case of a long

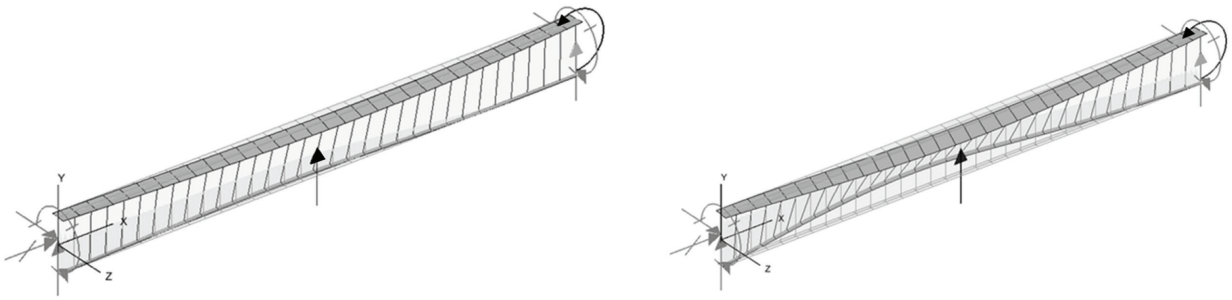

(a) $\xi = -0.4$ *(b)* $\xi = -0.5$

Fig. 21. Buckling mode shapes for $L_b/h_o = 10$, $J = 0$, $\rho = 0.9$, $\alpha = 0.0$, *concentrated transverse load, with* $\xi = -0.5$ *versus* $\xi = -0.4$; *applied loads are indicated by black arrows, reactions are indicated by grey arrows.*

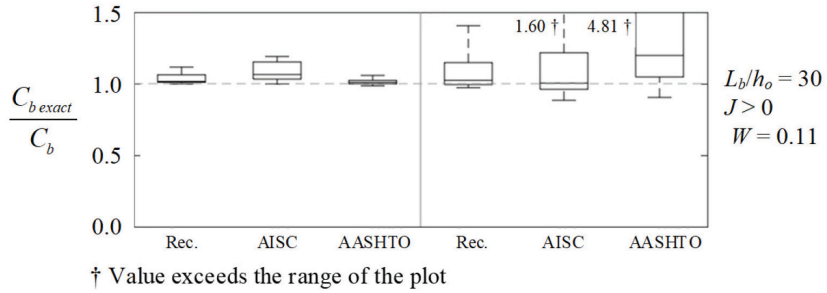

(a) Linear moment *(b) Nonlinear moment*

Fig. 22. Boxplots of $C_{b\,exact}/C_b$ *considering* W14×873 *members.*

heavy column to investigate the behavior of the C_b design estimates for this practical extreme.

Figure 22 shows boxplots for linear and nonlinear moment studies of the W14×873 members. For the linear moment studies, the AASHTO procedure clearly gives the best accuracy, while the recommended method provides a mean $C_{b\,exact}/C_{b\,Rec}$ of 1.03 and a COV of 0.034. The AISC *Specification* Equation F1-1 calculation is, on average, 9% conservative and has the largest COV of 0.055. The recommended method provides the best accuracy for the nonlinear moment cases, giving a mean $C_{b\,exact}/C_{b\,Rec}$ of only 1.05 and a COV of 0.084. The AISC *Specification* Equation F1-1 has a similar mean of 1.06 in these cases but a higher COV of 0.125. However, the recommended calculation never gives a $C_{b\,exact}/C_{b\,Rec}$ less than 0.972, whereas $C_{b\,exact}/C_{b\,AISC}$ is as small as 0.884.

SUMMARY AND CONCLUSIONS

This paper has presented a comprehensive evaluation of the results from the moment gradient factor (C_b) equations in the AISC (2016) *Specification* Commentary (ASC) and the AASHTO (2020) *Specifications* for prismatic singly symmetric I-section members. The investigation reveals that the ASC procedure produces both grossly conservative as well as significantly unconservative results in numerous practical situations. The causes of this behavior lie in the fact that the ASC quarter-point C_b equation is blind to the sign of the bending moment. The ASC calculation does not recognize the influence of different patterns of compression and tension in the different size flanges of a singly symmetric I-section member subjected to moment reversal. Furthermore, the ASC calculation exhibits substantial discontinuities in its C_b values as a function of the loading considered. This is due to its R_m factor. In recent developments, Reichenbach et al. (2020) recommend additional conditions on the application of R_m in the ASC C_b equation for members under reverse-curvature bending. These recommendations are considered in Appendix A. This modified ASC procedure gives improved results for a limited subset of specific cases but continues to show significant errors in general.

The C_b equations in the AASHTO *Specifications* provide some accounting for the different patterns of compression and tension in the separate flanges of singly symmetric I-section members subjected to moment reversal. However, these equations are based only on the moments at the ends and at the middle of the unbraced length. Hence, they are limited in their ability to capture the influence of nonlinear variations in moment along the unbraced length. In addition, the AASHTO procedure uses $C_b = 1.0$ in situations where the corresponding moment within the unbraced length is larger than the maximum brace point moment, causing compression in the flange under consideration. Furthermore, the AASHTO calculation can give significant discontinuities in the calculated C_b as a function of the loading considered. This is due to changes in the governing flange in its procedure and can produce substantially conservative results in certain cases.

To rectify the limitations of the current ASC and AASHTO methods, a modified form of an alternative quarter-point C_b equation proposed by Wong and Driver (2010) is recommended. For cases involving moment reversal within the unbraced length of singly symmetric members, the moment terms in the Wong and Driver equation are replaced by the ratio of the moments to the corresponding elastic buckling moment based on $C_b = 1$ (i.e., M/M_{cr1}), considering the flange that is in compression at each of the locations where the moments are sampled. The studies show that the Wong and Driver equation, with this modification, provides substantially improved accuracy compared to the current AASHTO and ASC methods. With respect to the current ASC equations:

- For singly symmetric members where the moment diagrams are close to linear, the recommended approach gives C_b values that are, on average, 25% larger than the ASC Equation CF1-3, and with a tighter COV on $C_{b\,exact}/C_b$ (0.104 vs. 0.569).
- For singly symmetric members with nonlinear moment diagrams, due to transverse loading with the unbraced length, the recommended approach gives C_b values that are on average 12% larger than the ASC Equation C-F1-3, again with a tighter COV on $C_{b\,exact}/C_b$ (0.191 vs. 0.344).
- Unconservative $C_{b\,exact}/C_b$ values, illustrated by a specific example to be as small as 0.466, corresponding to $C_{b\,exact} = 1.30$ while $C_{b\,ASC} = 2.79$, are avoided.

In addition, substantial conservatism of the AASHTO provisions, particularly for single-curvature cases where $C_{b\,AASHTO}$ is taken equal to 1.0 when $C_{b\,exact}$ is significantly larger than 1.0, is eliminated.

These improvements are achieved with a small reduction in the overall calculation effort relative to the current methods since the calculations of R_m in the ASC procedure and multiple C_b values in the AASHTO procedure are avoided. This aspect of the recommended method is highlighted by a practical design example in Appendix B.

In addition, the present studies show that the recommended equations do not require any cap on the maximum value of C_b obtained from the application of the actual and modified Wong and Driver quarter-point equations. As illustrated in the Background section of this paper and demonstrated further by Slein et al. (2021), the recommended equations show moderate improvements relative to the current AISC and AASHTO equations in benchmark solutions for doubly symmetric I-sections. Therefore, the Wong and Driver quarter-point equation, with the recommended modification to address singly symmetric I-section members

subjected to reverse-curvature bending, can be recommended as a simple single approach that can be applied to all routine situations involving moment gradient loading on I-section member unbraced lengths.

Lastly, the studies presented in the paper indirectly and independently confirm the findings from Helwig et al. (1997) that the web mid-height serves as the appropriate reference position on the cross-section profile from which load-height effects should be calculated, where appropriate. In all the studies conducted in this research, the transverse loads are applied at the web mid-height. The authors observed that this load position through the depth of the cross section clearly results in the best correlation between benchmark solutions and the predictions from the C_b equations targeted at singly symmetric I-section members. Furthermore, the studies in this paper provide independent confirmation of the benchmark results collected by Wong and Driver for specific doubly symmetric member cases.

As noted in the Introduction to the paper, the consideration of load-height effects, where appropriate, is an advanced topic that is commonly not addressed directly within design specifications. Readers are referred to Helwig et al. for detailed consideration of load-height effects. The practical C_b equation modifications recommended by Helwig et al. are considered applicable with the recommended base C_b equations presented in this paper. In addition, as discussed in the Introduction to the paper, the degree of lateral, rotational, and warping restraint provided at the ends of unbraced lengths, including continuity with and buckling interaction with adjacent unbraced segments, is not considered in the evaluation of the C_b procedures in this paper. Software such as SABRE2 (White et al., 2021), which has been employed to generate the benchmark solutions presented in this paper, provides one advanced option that allows these attributes to be readily addressed. Other general loading and boundary condition effects such as discussed by Wong and Driver (e.g., members with concentrated applied moments within their lengths), unbraced cantilevers with fixed supports or with flexible back-spans, etc., where manual estimates can become more challenging, can be readily addressed by modern computational methods such those as provided in SABRE2.

APPENDIX A

Recent Improvements to the ASC Method in the Literature

Reichenbach et al. (2020) recently recommended additional conditional requirements for the application of R_m in the ASC C_b equation for members under reverse-curvature bending. Reichenbach et al. specify in their Equation 10 that R_m should be taken equal to 1.0 for cases in which both $-0.5 < M_{small}/M_{large} < 0$ and $x_{inf} \leq 0.375L_b$, where M_{small} and M_{large} are the smaller and larger end moments on the unbraced length, and x_{inf} is the distance between the inflection point and the braced end corresponding to M_{small}.

Therefore, in the modified approach recommended by these authors,

$$R_m = 1.0 \tag{A-1a}$$

for (1) doubly symmetric members; (2) singly symmetric members subjected to single-curvature bending; and (3) singly symmetric members subjected to reverse-curvature bending when both the ratio of the end moments is between 0 and −0.5, exclusive, and the inflection point is located within $0.375L_b$ of the braced end with the smallest end moment in magnitude, inclusive. Otherwise,

$$R_m = 0.5 + 2\left(\frac{I_{y.opp}}{I_y}\right)^2 \tag{A-1b}$$

The ratio of M_{small}/M_{large} is directly related to the term α. The limit $-0.5 < M_{small}/M_{large} < 0$ corresponds to $-0.5 < \alpha < 0$ and $\alpha < -2.0$. In the parametric study cases presented in the current paper, α ranges between −1.0 and 1.0 for nonlinear moment diagrams and between −5.0 and 1.0 for linear moment diagram cases. For the linear moment diagram cases (e.g., see Figure 7), the results are plotted at a small increment in α such that the plots are effectively continuous; however, the nonlinear moment diagram cases are evaluated at $\alpha = -1.0$, −0.5, 0.0, 0.5, and 1.0. As such, when the modifications to R_m recommended by Reichenbach et al. are applied to the studies in this paper, there is no change in the results for the nonlinear moment diagram cases. Furthermore, for the linear moment diagram cases, the $0.375L_b$ limit on the inflection point location corresponds to $M_{small}/M_{large} = -0.6$, so the condition on the inflection point is always satisfied. Therefore, in effect, only the limits on α apply.

To evaluate the performance of the modified procedure recommended by Reichenbach et al. (2020) in the limit of linear moment diagrams, Figure A-1 is considered. This figure is an adaptation of Figure 15 in which the AASHTO results are replaced by the results from the modified ASC method recommended by Reichenbach et al. (2020), labeled as ASC*. Figure A-1 shows improvements by neglecting R_m when $-0.5 < \alpha < 0$ and $\alpha < -2.0$; however, for $-2.0 \leq \alpha \leq 0.5$, the ASC* procedure uses the same R_m as the ASC method, resulting in $C_{b\,exact}/C_{b\,ASC*}$ as small as 0.710, or a 40.8% overestimation. Furthermore, it is important to note that there are two discrete shifts in $C_{b\,ASC*}$ instead of the one discrete shift in $C_{b\,ASC}$ in Figure 15(a).

In Figure A-1(a), the behavior of R_m as a function of α in the ASC* method is as follows:

- For $\alpha \geq 0$, $R_m = 1.0$ due to single-curvature bending.
- For $-0.5 < \alpha < 0$, $R_m = 1.0$ since $-0.5 < M_{small}/M_{large} < 0$. The particulars for $\alpha = -0.49$, labeled as Case 11, are shown in Figure A-1(d).
- For $-1.0 \leq \alpha \leq -0.5$, $R_m = 2.118$ since $M_{small}/M_{large} \leq -0.5$. The particulars for $\alpha = -0.51$, labeled as Case 10, are shown in Figure A.-1(c).
- For $-2.0 < \alpha \leq -1.0$, $R_m = 2.118$ since M_{small}/M_{large} is less than -0.5 (note that left end moment now has the larger magnitude). The particulars for $\alpha = -1.99$, labeled as Case 9, are shown in Figure A-1(b).
- For $\alpha < -2.0$, $R_m = 1.0$ since $-0.5 < M_{small}/M_{large} < 0$.

These cases demonstrate that the recommendations by Reichenbach et al. (2020) do improve the results within a portion of the design space; however, the results are still highly inaccurate elsewhere.

Figure A-2 is an adaptation of Figure 16, where again the results for the AASHTO methodology are replaced with the results based on the ASC* method recommended by Reichenbach et al. (2020). Figure A-2(a) shows that the updated ASC methodology fixes the unconservative error illustrated in Figure 16(a). However, it does not fix the conservative error. In the plot in Figure A-2(a), R_m is included once the inflection point moves within $0.375L_b$ from the location of M_{small}. This occurs at $\xi \leq -0.050$. This inclusion of R_m results in $C_{b\ exact}/C_{b\ ASC*}$ values as large as 2.11. Figure A-2(b) shows the particulars for Case 12, exhibiting the largest error.

Figure A-3(a) has the same loadings as Figure A-2(a), but ρ is changed from 0.9 to 0.1. In Figure A-3(a), the updated methodology fixes the conservative errors, but it does not fix the unconservative errors. Figure A-3(b) shows the worst case, Case 13, where $C_{b\ exact}/C_{b\ ASC*} = 0.497$, with the ASC* procedure overpredicting by more than a factor of 2.0.

Based on the results illustrated in Figures A-1, A-2, and A-3, it is apparent that further adjustments would be needed to the ASC* procedure to limit the large conservative and unconservative errors still exhibited. The recommended adaptation of the Wong and Driver procedure presented in the current paper avoids the complexities of the various conditional tests associated with the ASC* method while maintaining simplicity of the calculations and giving an accurate estimate of the benchmark C_b.

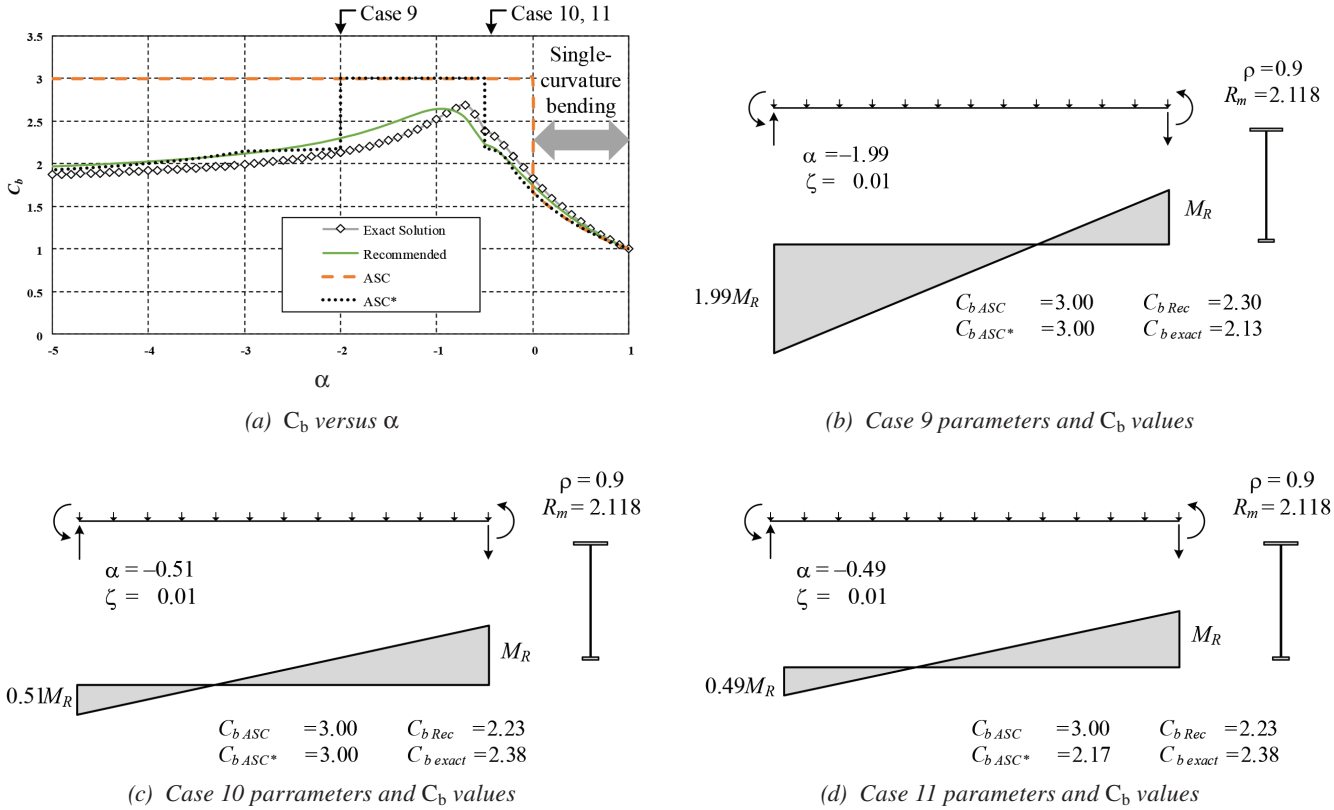

(a) C_b *versus* α

(b) Case 9 parameters and C_b *values*

(c) Case 10 parrameters and C_b *values*

(d) Case 11 parameters and C_b *values*

Fig. A-1. Cases exhibiting smallest $C_{b\ exact}/C_b$ *for the ASC, ASC* (Reichenbach et al., 2020) and recommended procedures for linear moment:* $L_b/h_o = 30$, $\rho = 0.9$ ($C_{b\ exact}/C_{b\ ASC} = 0.608$ *at* $\alpha = 0$, $C_{b\ exact}/C_{b\ ASC*} = 0.710$ *at* $\alpha = -1.99$, $C_{b\ exact}/C_{b\ Rec} = 0.920$ *at* $\alpha = -1.5$).

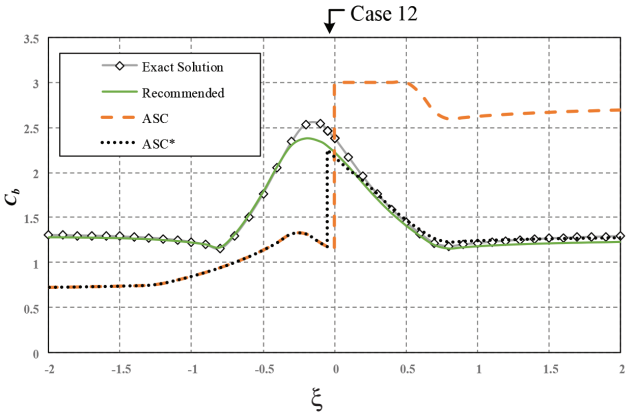

(a) C_b *versus* ξ

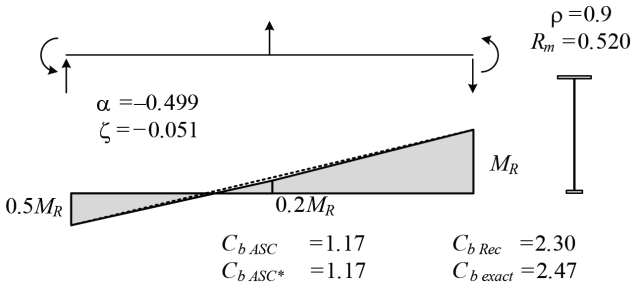

(b) Case 12 parrameters and C_b *values*

Fig. A-2. Partially improved performance of $C_{b\,exact}/C_b$ *for the modified ASC procedure recommended by Reichenbach et al. (2020), nonlinear moment—Case 12: concentrated transverse load,* $L_b/h_o = 30$, $\rho = 0.9$, $\alpha = -0.499$ ($C_{b\,exact}/C_{b\,ASC*} = 2.11$ *at* $\xi = -0.051$).

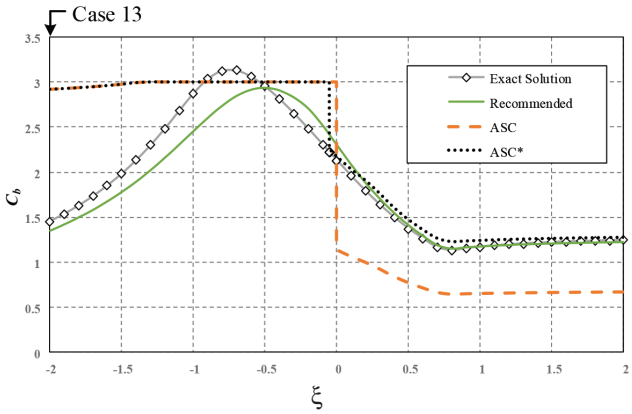

(a) C_b *versus* ξ

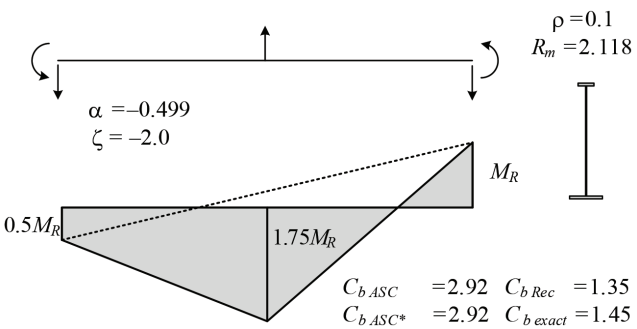

(b) Case 12 parrameters and C_b *values*

Fig. A-3. Worst-case $C_{b\,exact}/C_b$ *for the modified ASC procedure recommended by Reichenbach et al. (2020), nonlinear moment—Case 13: concentrated transverse load,* $L_b/h_o = 30$, $\rho = 0.1$, $\alpha = -0.499$ ($C_{b\,exact}/C_{b\,ASC*} = 0.497$ *at* $\xi = -2.0$).

APPENDIX B

Reverse-Curvature Bending Design Example

The following example design calculations consider a two-span continuous bridge girder with equal span lengths. The focus of the calculations is on determining the distributed load the girder can safely support during construction, considering the LTB limit state. It is assumed that the girder is braced at the abutments, at the pier section, and at each mid-span location. It is assumed that form supports distribute a portion of the load to the bottom flange; therefore, mid-height loading is assumed as in the example presented by Helwig et al. (1987).

The girder cross section is the same as the cross section considered in example design calculations by Helwig et al. (1987), except all the dimensions are scaled by a factor of 1.5. This gives a 12 in. × 1.5 in. top flange, an 18 in. × 1.5 in. bottom flange, and a 60 in. × 0.75 in. web. The span length of the girder is taken as 150 ft, giving an unbraced length of $L_b = 75$ ft.

Load and resistance factors are not included in the calculations.

This problem has some similarity to the Case 7 example shown in Figure 19, except the monosymmetry is not as severe in this problem ($\rho = 0.229$) and the length-to-depth ratio of the unbraced length is smaller ($L_b/h_o = 15$). Figure B-1 shows the moment diagram for the right-hand span, with the pier section located on the left-hand end of the span. The unbraced length under consideration is the one subjected to reverse-curvature bending adjacent to the pier. The maximum negative and positive moments as well as the quarter-point moments are labeled in the figure. The moment diagram in the subject unbraced length corresponds to $\alpha = -2.0$ and $\xi = +0.5$.

The following calculations are the same for the three methods being evaluated:

$$r_{t.top} = \frac{b_{f.top}}{\sqrt{12\left(1+\frac{1}{3}\frac{D_{c.top}t_w}{b_{f.top}t_{f.top}}\right)}} = 2.87$$

$$r_{t.bot} = \frac{b_{f.bot}}{\sqrt{12\left(1+\frac{1}{3}\frac{D_{c.bot}t_w}{b_{f.bot}t_{f.top}}\right)}} = 4.65$$

$$M_{cr1.top} = \frac{\pi^2 E S_{xc.top}}{\left(\frac{L_b}{r_{t.top}}\right)^2}\sqrt{1+0.078\frac{J}{S_{xc.top}h_o}\left(\frac{L_b}{r_{t.top}}\right)^2}$$

$$= 788 \text{ kip-ft}$$

$$M_{cr1.bot} = \frac{\pi^2 E S_{xc.bot}}{\left(\frac{L_b}{r_{t.bot}}\right)^2}\sqrt{1+0.078\frac{J}{S_{xc.bot}h_o}\left(\frac{L_b}{r_{t.bot}}\right)^2}$$

$$= 1{,}740 \text{ kip-ft}$$

The calculations for the three primary methods evaluated in the paper are presented in the following subsections and are compared to a converged numerical benchmark solution of the distributed load the girder can safely support during construction of $\gamma_{e.exact}(1 \text{ kip/ft}) = 1.38$ kip/ft from SABRE2 (White et al., 2021).

ASC and ASC* Procedures

For the ASC* procedure, the updated exclusion criteria for the calculation of R_m,

$$M_{small}/M_{large} < -0.5 \qquad x_{inf} \le 0.375L_b \text{ from } M_{small}$$

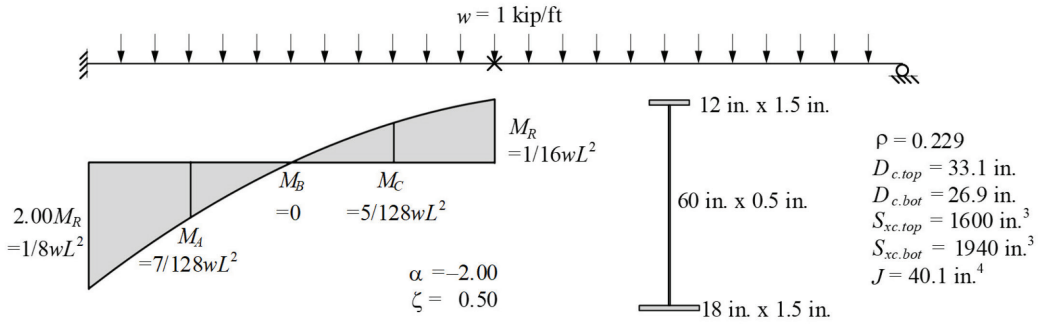

Fig. B-1. Moment diagram and cross-section properties for an example bridge girder during construction having $L_b/h_o = 15$, $\rho = 0.229$, $\alpha = -2.0$, *and* $= +0.5$.

are violated for this example. Therefore, R_m is calculated using Equation 1b and the ASC* method gives the same result as the ASC method:

$$R_m = 0.5 + 2\left(\frac{I_{y.top}}{I_y}\right)^2 = 0.604$$

$$C_b = \frac{12.5M_{max}}{2.5M_{max} + 3M_A + 4M_B + 3M_C} R_m = 1.59 \le 3.0$$

Using Equation 2, considering the largest moment and the base elastic buckling capacities associated with each flange, the elastic buckling load ratio is calculated as

$$\gamma_{eLTB} = \min\left(\frac{C_b M_{cr1.top}}{M_{max.top}}, \frac{C_b M_{cr1.bot}}{M_{max.bot}}\right) = 0.890$$

$$w_{cr} = \gamma_{eLTB}(1 \text{ kip/ft}) = 0.890 \text{ kip/ft}$$

The resulting distributed load the girder can safely support during construction through the ASC and ASC* procedure is highly conservative, at 64% of the benchmark solution. Note that if R_m were taken equal to 1.0, the resulting distributed load the girder can safely support is estimated as 1.47 kip/ft, or approximately 6.5% larger than the benchmark solution.

AASHTO Procedure

For reverse-curvature bending cases, the AASHTO procedure requires assessment of the concavity or convexity the moment diagram with respect to each flange. Using Equations 8 and 9, the moment gradient factors for each flange are calculated as

$$C_{b.bot} = \min\left[1.75 - 1.05\frac{M_0}{M_2} + 0.3\left(\frac{M_0}{M_2}\right)^2, 2.5\right] = 2.35$$

$$C_{b.top} = \min\left[3.10 - 3.30\frac{M_{mid}}{M_2} + 1.2\left(\frac{M_{mid}}{M_2}\right)^2, 2.5\right] = 2.5$$

Using Equation 7, considering the respective moment gradient factor, largest moment, and elastic buckling capacity in each flange, the elastic buckling load ratio is calculated as

$$\gamma_{e.AASHTO} = \min\left(\frac{C_{b.top} M_{cr1.top}}{M_{max.top}}, \frac{C_{b.bot} M_{cr1.bot}}{M_{max.bot}}\right) = 1.40$$

$$w_{cr} = \gamma_{eLTB}(1 \text{ kip/ft}) = 1.40 \text{ kip/ft}$$

The resulting distributed load the girder can safely support through the AASHTO procedure is slightly unconservative, 1.4% larger than the benchmark solution.

Recommended Procedure

The recommended procedure considers the ratios of the moment demands to the critical elastic moment of the flange in compression, either $M_{cr1.top}$ or $M_{cr1.bot}$, along the length of the member.

$$C_b = \frac{4\left(\frac{M}{M_{cr1}}\right)_{max}}{\sqrt{\left(\frac{M}{M_{cr1}}\right)^2_{max} + 4\left(\frac{M}{M_{cr1}}\right)^2_A + 7\left(\frac{M}{M_{cr1}}\right)^2_B + 4\left(\frac{M}{M_{cr1}}\right)^2_C}} = 2.24$$

Using Equation 11, the elastic buckling load ratio is calculated as

$$\gamma_{e.Recommended} = \frac{C_b}{\left(\frac{M}{M_{cr1}}\right)_{max}} = 1.26$$

$$w_{cr} = \gamma_{eLTB}(1 \text{ kip/ft}) = 1.26 \text{ kip/ft}$$

The resulting distributed load the girder can safely support through the recommended procedure is slightly conservative, at approximately 91% of the benchmark solution.

REFERENCES

AASHTO (2020), *AASHTO LRFD Bridge Design Specifications*, 9th Ed., American Association of State and Highway Transportation Officials, Washington, D.C.

AISC (2016), *Specification for Structural Steel Buildings and Commentary*, ANSI/AISC 360-16, American Institute of Steel Construction, Chicago, Ill.

Helwig, T.A., Frank, K.H., and Yura, J.A. (1997), "Lateral-Torsional Buckling of Singly-Symmetric I-Beams," *Journal of Structural Engineering*, ASCE, Vol. 123, No. 9, pp. 1,172–1,179.

Jeong, W.Y. (2014), "Structural Analysis and Optimized Design of General Nonprismatic I-Section Members," Doctoral Dissertation, Georgia Institute of Technology, Atlanta, Ga.

Kitipornchai, S., Wang, C.M., and Trahair, N.S. (1986), "Buckling Properties of Monosymmetric I-Beams under Moment Gradient," *Journal of Structural Engineering*, ASCE, Vol. 112, No. 4, pp. 781–799.

Reichenbach, R.C., Liu, Y., Helwig, T.A., and Engelhardt, M.D. (2020), "Lateral-Torsional Buckling of Singly-Symmetric I-Girders with Stepped Flanges," *Journal of Structural Engineering*, ASCE, doi:10.1061/(ASCE)ST.1943-541X.0002780.

Salvadori, M.G. (1956), "Lateral Buckling of I-Beams," *ASCE Transactions*, American Society of Civil Engineers, Vol. 120, pp. 1,165–1,177.

Slein, R., Jeong, W.Y., and White, D.W. (2021), "A Critical Evaluation of Moment Gradient (C_b) Factor Calculation Procedures for Singly Symmetric I-Section Members," Structural Engineering, Mechanics and Materials Report No. 5, School of Civil and Environmental Engineering, Georgia Institute of Technology, Atlanta, Ga.

White, D.W., Slein, R., Toğay, O., and Jeong, W.Y. (2021), "SABRE 2," white.ce.gatech.edu/sabre (August 31, 2021).

Wong, E. and Driver, R. (2010), "Critical Evaluation of Equivalent Moment Factor Procedures for Laterally Unsupported Beams," *Engineering Journal*, AISC, Vol. 47, No. 1, pp. 1–20, and Closure, Vol. 47, No. 4, pp. 281–283.

Ziemian, R. (2010), *Guide to Stability Design Criteria for Metal Structures*, 6th Ed., Wiley, N.Y.